

# Title

Multi-scale hierarchical neural network models that bridge from single neurons in the primate primary visual cortex to object recognition behavior

# Authors

Tiago Marques<sup>1,2\*</sup>, Martin Schrimpf<sup>1,2</sup> and James J. DiCarlo<sup>1,2</sup>

1. McGovern Institute for Brain Research and Department of Brain and Cognitive Sciences, Massachusetts Institute of Technology, Cambridge, MA, 01239, USA

2. Center for Brains, Minds, and Machines, Massachusetts Institute of Technology, Cambridge, MA, 01239, USA

# Correspondence

\*Correspondence should be addressed to Tiago Marques.

# Contact Info

McGovern Institute for Brain Research  
Massachusetts Institute of Technology,  
77 Massachusetts Institute of Technology, 46-6161,  
Cambridge, MA 02139  
E-mail: [tmarques@mit.edu](mailto:tmarques@mit.edu)

# Highlights

- Single neurons in some image-computable hierarchical neural network models are functionally similar to single neurons in macaque primate visual cortex (V1)
- Some hierarchical neural networks models have V1 layers that better match the biological distributions of macaque V1 single neuron response properties
- Multi-stage hierarchical neural network models with V1 stages that better match macaque V1 are also more aligned with human object recognition behavior at their output stage

# Abstract

Object recognition relies on inferior temporal (IT) cortical neural population representations that are themselves computed by a hierarchical network of feedforward and recurrently connected neural population called the ventral visual stream (areas V1, V2, V4 and IT). While recent work has created some reasonably accurate image-computable hierarchical neural network models of those neural stages, those models do not yet bridge between the properties of individual neurons and the overall emergent behavior of the ventral stream. For example, current leading ventral stream models do not allow us to ask questions such as: How does the surround suppression behavior of individual V1 neurons ultimately relate to IT neural representation and to behavior?; or How would deactivation of a particular sub-population of V1 neurons specifically alter object recognition behavior? One reason we cannot yet do this is that individual V1 artificial neurons in multi-stage models have not been shown to be functionally similar with individual biological V1 neurons. Here, we took an important first step towards this direction by building and evaluating hundreds of hierarchical neural network models in how well their artificial single neurons approximate macaque primary visual cortical (V1) neurons. We found that single neurons in some models are surprisingly similar to their biological counterparts and that the distributions of single neuron properties, such as those related to orientation and spatial frequency tuning, approximately match those in macaque V1. Crucially, we also observed that hierarchical models with V1-layers that better match macaque V1 at the single neuron level are also more aligned with human object recognition behavior. These results provide the first multi-stage, multi-scale models that allow our field to ask precisely how the specific properties of individual V1 neurons relate to recognition behavior. Finally, we here show that an optimized classical neuroscientific model of V1 is still more functionally similar to primate V1 than all of the tested multi-stage models, suggesting that further model improvements are possible, and that those improvements would likely have tangible payoffs in terms of behavioral prediction accuracy and behavioral robustness.

# Keywords

primary visual cortex, object recognition, hierarchical neural network models, single neuron properties, primate vision

# Introduction

The primate ventral visual stream, a network of hierarchically-organized cortical areas, has been shown to support visually-guided behaviors (Felleman & Van Essen, 1991; Mishkin, Ungerleider, & Macko, 1983). One such particularly important behavior is core object recognition -- i.e., the ability to rapidly (~200ms) identify objects in the central visual field (DiCarlo, Zoccolan, & Rust, 2012; Fabre-Thorpe, Richard, & Thorpe, 1998). Understanding the computations and neuronal mechanisms underlying this complex visual behavior has been a major goal in systems neuroscience (DiCarlo & Cox, 2007). A critical step towards this goal is the development of accurate, multi-stage, multi-scale models that can bridge between the properties of individual cells and phenomena at each of the ventral stream processing stages to the supported visually-guided behaviors, such as core recognition. These multi-stage, multi-scale models would, for example, allow us to begin to understand how functional properties at the cellular level, where we can most conveniently measure and manipulate the system, give rise to complex cognitive phenomena such as visually intelligent behavior. Successful multi-scale models must be simultaneously accurate at both the individual neuron level, at the neuronal population level, and at the behavioral level. The work presented here is one step toward that greater goal.

Prior work has shown that hierarchical networks of artificial neural populations can, when properly connected, quite closely approximate object recognition behavioral patterns that are driven by the ventral visual stream, a similarly organized deep hierarchy of biological neurons (Rishi Rajalingham et al., 2018). In addition, this same model family has achieved unparalleled success in explaining the response patterns of individual neurons along the ventral stream areas (Bashivan, Kar, & DiCarlo, 2019; Cadena et al., 2019; Kar, Kubilius, Schmidt, Issa, & DiCarlo, 2019; Schrimpf et al., 2018; Yamins et al., 2014). Thus, we and others have proposed that these models may serve as multi-stage, multi-scale models of the mechanisms of object recognition -- bridging from single neuron responses at multiple stages of the ventral stream to the observed recognition behavioral patterns (Kriegeskorte, 2015; Richards et al., 2019; Schrimpf et al., 2020; Yamins & DiCarlo, 2016). However, this model to brain congruency has not been without criticism. In particular, these models often have thousands of features which are linearly combined to explain the responses of neurons (Saxe, Nelli, & Summerfield, 2021; Serre, 2019). The existence of this fitting step means that hierarchical neural networks may not be accurate multi-scale models of the neural mechanisms of object recognition since the congruency tests typically do not require that the individual artificial single neurons are aligned with individual biological neurons within the proposed congruent cortical area(s).

To address this limitation, we here hypothesized that these hierarchical models of artificial neurons might be modified to become accurate, multi-scale models of the neural mechanisms of visual object recognition. To investigate this, we made a more explicit one-to-one mapping commitment between artificial neurons in these hierarchical models and biological neurons in the primate primary visual cortex (area V1). Specifically, we bypassed the usual model-to-brain fitting procedure and we sought to test the hypothesis that single neurons in a candidate model layer (i.e. a specific processing stage of a candidate hierarchical model) correspond to single neurons in the macaque V1, and that the entire artificial neural population at that same model layer corresponds to the entire

V1 neuronal population. We were encouraged to pursue this approach to modeling V1 neurons in part because of prior work demonstrating that one such hierarchical network model contains neural representations which, when linearly combined using a regression approach, can reasonably accurately predict the response patterns of V1 (Cadena et al., 2019).

To explore this single model neuron-to-single brain neuron hypothesis, we performed in-silico neurophysiological experiments in hundreds of these V1 candidate models to measure 22 single neuron response properties that have been previously quantified, such as those related to orientation and spatial frequency tuning and surround and texture modulation, and compared their distributions to those in macaque V1 from available published studies (Cavanaugh, Bair, & Movshon, 2002; De Valois, Albrecht, & Thorell, 1982; De Valois, Yund, & Hepler, 1982; Freeman, Ziemba, Heeger, Simoncelli, & Movshon, 2013; Ringach, Shapley, & Hawken, 2002; P. H. Schiller, Finlay, & Volman, 1976; Ziemba, Freeman, Movshon, & Simoncelli, 2016).

Indeed, we found that single artificial neurons in the V1-layers of some hierarchical models did indeed already have response characteristics that were surprisingly similar to those of single neurons in macaque V1, and, moreover, we also found that the distributions of response properties also very closely matched their biological counterparts. Since all of these hierarchical models were also candidate models of the entire ventral stream and its supported object recognition behavior, we then went on to ask: Do ventral stream models that better align with biological V1 at their putative V1 processing stage also better align with the behavioral patterns of human core object recognition? Indeed, we found that hierarchical models with V1-layers that better approximated macaque V1 at the level of single neurons, were more aligned with human behavior. Thus, this work demonstrates, for the first time, implemented, image-computable, multi-stage models of the primate visual ventral stream that reasonably bridge from the level of single neurons in V1, the first visual cortical area, all the way to object recognition behavior.

Still, we also found that no evaluated ventral stream model was able to perfectly account for all the V1 response properties and underperformed when compared to an optimized classical neuroscientific model that was built only to explain V1 response properties. This shows that the multi-scale models of the ventral stream developed here can be further improved, and argues that improvements -- even at just the earliest processing stage -- will lead to better alignment with human object recognition behavior.

## Results

Our overarching goal is to build accurate, multi-stage, multi-scale models of the ventral visual stream. By definition, such models must be accurate at the level of single neurons, at the levels of populations of such neurons, at all ventral stream stages, and for all ventral stream behaviors. In this work, we focus on primate visual area V1 and we evaluate how well specific hierarchical artificial neural networks (ANNs), some of which are the current leading models of the ventral visual stream (Cadena et al., 2019; Kubilius et al., 2019; Schrimpf et al., 2018; Yamins et al., 2014), directly align at the level of V1 single neurons.

We used this approach to study how next generations of ventral stream models might be made to better align at the V1 stage and to also ask how V1 individual neuronal response properties relate to object recognition behavior. Contrary to prior approaches that used fitting high dimensional feature spaces in the models to the responses of relatively small neuronal populations (Cadena et al., 2019) we here tested the even stronger hypothesis that single neurons in variants of the existing hierarchical ventral stream models may qualitatively and quantitatively align with single neuron functional properties in macaque V1 in a one-to-one manner (see Fig. 1, bottom).

To test this hypothesis, we developed a three-step approach for building hundreds of candidate models of V1 using specific, hierarchical ANNs that are already among the leading models of the ventral visual stream (Figure 1, top). First, we choose a base model consisting of a hierarchical network architecture and all its synaptic weights which are typically obtained by standard training using the object classification ImageNet dataset, though we also used models with their weights optimized differently (see Methods). Second, since the base model's input is solely defined by its resolution in pixels (the model's input sensors, 224x224 in all the models used) with no connection to physical quantities, we specified the region of visual space (in degrees) that corresponds to the model's input and we termed that the field-of-view (FoV). In this study we considered multiple model FoV's. Relative to models with a smaller FoV, models with a larger FoV have the same number of input sensors, but those sensors sample over a larger spatial extent and each integrate over a correspondingly larger spatial extent. Third, we assign all the artificial neurons within a specific layer of the hierarchical model as a candidate model of the macaque V1 neural population. Due to the convolutional architecture of the neural networks used, each model layer consists of multiple feature spatial maps and thus each candidate V1 model contains  $w \times h \times d$  artificial neurons (range 10K-3M artificial neurons). To compare with biological data such that we assume a one-to-one mapping of artificial neurons with biological neurons, we discard information about each neuron's spatial location and feature number and treat it as a putative single neuron in foveal macaque V1. In other words, for each candidate V1 we randomly sample artificial neurons from this pool as if we were randomly sampling individual neurons with a recording electrode. We then quantify the response properties of these individually sampled artificial individual neurons, and make quantitative comparisons with the same measurements of individual biological V1 neurons from multiple such experiments.

In total, we considered: (1) 13 different base models including AlexNet (Krizhevsky, Sutskever, & Geoffrey E., 2012), VGG (Simonyan & Zisserman, 2015), ResNet (He, Zhang, Ren, & Sun, 2016), CORnet (Kubilius et al., 2019), and bagnet (Brendel & Bethge, 2019); (2) four different FoVs (between 4 and 10 degrees); and (3) multiple early and intermediate layers for each base model. This resulted in 736 candidate V1 models (see methods for a complete description).

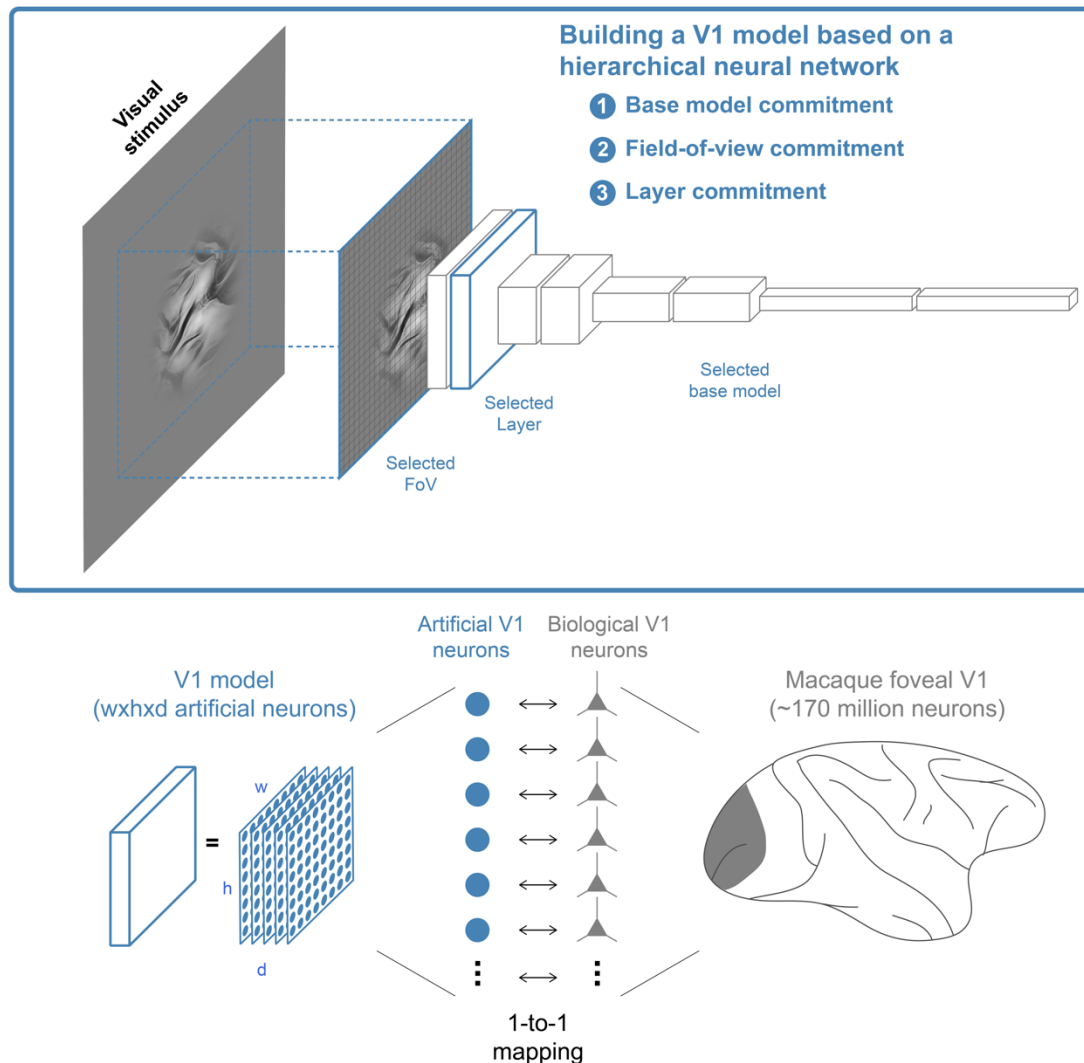


**Figure 1. Building V1 models at the level of single neurons using hierarchical neural networks.** Top, proposed methodology for building a candidate model of macaque V1 involves three steps: (1) the choice of a base model defined by its architecture and synaptic weights, (2) the choice of the field-of-view (FoV) in physical units (degrees), and (3) the choice of the processing stage, i.e. layer, to map to V1. Bottom, the model of V1 based on a hierarchical neural network is a convolutional layer containing  $w \times h \times d$  neurons, where  $w$ ,  $h$ , and  $d$ , are the width, height, and number of features, respectively. In this modeling framework there is an implied one-to-one mapping at the level of single neurons, that is, each artificial neuron in the model is assumed to correspond to a putative biological neuron that might have been recorded in macaque foveal V1.

## Single artificial neurons in some hierarchical networks have response patterns that are qualitatively similar to those of single neurons in macaque V1

Over the last several decades, responses of individual neurons in macaque V1 have been extensively characterized using different types of artificial stimuli such as gratings with varying phase, orientation, spatial frequency (SF) and size, and naturalistic textures and noise images (Figure 2B,C). Simple cells show responses strongly modulated by the phase of gratings while complex cells are invariant to this stimulus property (Skottun et al., 1991). Furthermore, V1 neurons vary widely in their orientation (De Valois, Yund, et al., 1982; Ringach et al., 2002; Peter H Schiller, Finlay, & Volman, 1976) and SF (De Valois, Albrecht, et al., 1982; P. H. Schiller et al., 1976) selectivities, RF sizes, and the



degree to which stimuli outside their RFs modulate their responses (Cavanaugh et al., 2002; H. E. Jones, Grieve, Wang, & Sillito, 2001; Kapadia, Ito, Gilbert, & Westheimer, 1995; Lamme, 1995; Sceniak, Ringach, Hawken, & Shapley, 1999). Finally, V1 neurons tend to respond similarly to texture stimuli and noise images with matching spatially averaged orientation and SF structure (Freeman et al., 2013; Ziemba et al., 2016). In prior experimental work, these characteristics of neuronal responses were quantified by calculating response properties (Figure 2C) such as: the F1/F0 ratio (ratio of the first harmonic and the DC component of responses to drifting gratings, also known as phase modulation ratio), preferred orientation and circular variance (CV; quantifies how selective the responses to different orientations are), peak SF and SF bandwidth, grating summation field (GSF; size of the stimulus for which the response is maximized; related to the size of the excitatory component of the RF) and surround suppression index (SSI, quantifies how much responses are suppressed by stimuli outside the classical RF), and texture modulation index (TMI, quantifies how much stronger neurons respond to naturalistic textures versus noise images).

Using the V1 candidate models previously described, we performed a series of *in silico* recordings to characterize the responses of their single neurons. After mapping the RFs of individual neurons by presenting small gratings at different locations (Figure 2A; methods), we recorded their visual responses to the presentation of stimuli typically used to study macaque V1 (Figure 2D). We found that single neurons in some V1 candidate models show responses to visual stimuli that are similar to those in macaque V1, allowing us to calculate response properties exactly the same way as with neurophysiology data (Figure 2D). Like in macaque V1, single artificial neurons within the same V1 model vary widely in their responses. For example, they vary in their selectivity to phase, orientation, and SF of gratings, RF size, and in how their responses are inhibited by the presence of surrounding stimuli (Figure 2D).

In addition to this intra-model variability, we found that median single neuron response properties also vary considerably across alternative candidate V1 models. This variation is driven by the base model choice, the FoV choice, and the layer choice (Supplementary Figure 1). Some response properties vary with these V1 model choices in an obvious and intuitive way. For example, a V1 model's median neuronal RF size (GSF) increases with both the layer choice and the FoV choice: V1 candidate models selected from deep layers contain neurons that can potentially integrate input from larger portions of the visual field (relative to more shallow layers), and V1 candidate models with larger FoVs can potentially integrate over larger portions of visual space as measured in degrees (Supplementary Figure 1). Similarly, a V1 model's median neuronal peak spatial frequency decreases with increasing FoV. On the other hand, other response properties show strong dependences on model properties that are not as intuitive. For example, surround suppression and texture modulation indices vary considerably with layer depth (Supplementary Figure 1). Surround suppression in particular is a key property of macaque V1 that is thought to be mediated by lateral and feedback connections (Bair, Cavanaugh, & Movshon, 2003; Nassi, Lomber, & Born, 2013; Nurminen, Merlin, Bijanzadeh, Federer, & Angelucci, 2018). Surprisingly, we observe that even in purely feedforward hierarchical neural network candidate V1 models, single artificial neurons also exhibit suppression of responses from surrounding stimuli (Figure 2D and Supplementary Figure 1).

These results thus far qualitatively demonstrate that despite their much simpler architecture when compared to cortical circuits, single artificial neurons in hierarchical neural network models respond to visual stimuli similarly to single macaque V1 neurons. Furthermore, response properties of single artificial neurons in these hierarchical models depend on different aspects of the model commitment to biology (e.g. assumed field of view), and, in some cases, in unexpected ways.

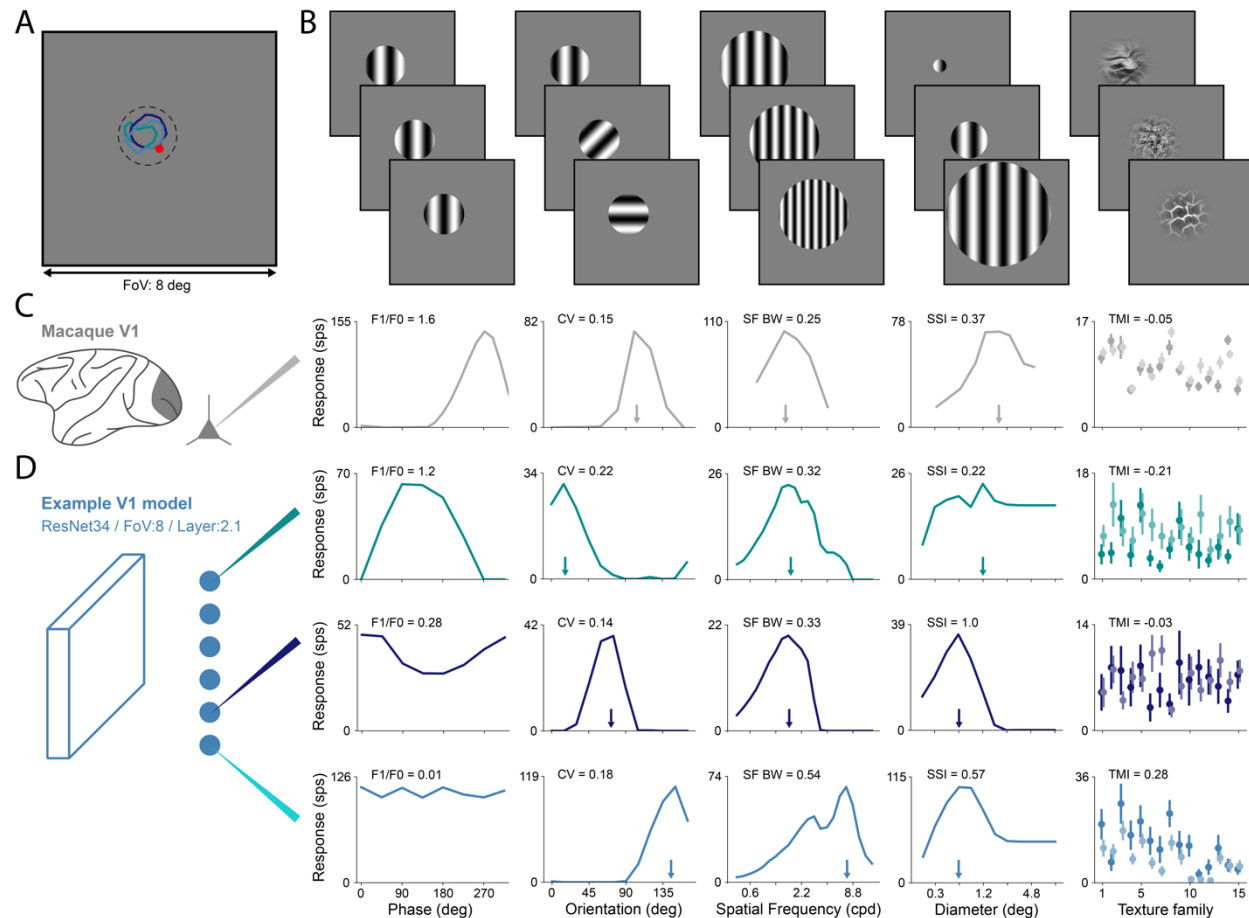


**Figure 2. Single neurons in some V1 models show responses similar to those of neurons in macaque V1.** **A.** Field-of-view of example V1 model with 8 deg. Red circle shows center of gaze. Dashed circle represents the location of a stimulus with a circular aperture (2deg diameter). Colored contours show the receptive field locations of three example neurons aligned with the stimulus center. **B.** Example stimuli used in the in silico neurophysiology characterization of single neurons in V1. From left to right: gratings with varying phase, gratings with varying orientation, gratings with varying spatial frequency, gratings with varying size, and naturalistic texture and noise images. **C.** Example responses of neurons in macaque V1. From left to right: phase, orientation, spatial frequency, and size tuning curves, and responses to naturalistic textures (dark tone) and spectrally matched noise images (light tone). Plots are vertically aligned with the corresponding example stimuli on **B**. Responses are taken from published studies and each plot corresponds to a different neuron. Example single neuron properties calculated from these responses are displayed at the top of each corresponding plot (phase modulation ratio, circular variance, spatial-frequency bandwidth, surround suppression index, and texture modulation index). Arrows indicate the preferred orientation, peak spatial frequency, and grating summation field in their respective plots. **D.** Similar to **C** but for three example neurons from a V1 model (ResNet34 base model, FoV of 8deg, and Layer2.1 as the V1-layer). The plots on each row correspond to the same neuron with the receptive field shown in **A** with matching color. Within the same layer of the hierarchical neural network model, single neurons exhibit very different responses characteristics. Neuron in the top row has a simple-cell like response with a strong phase modulation while the other two neurons show more complex-like responses. All neurons are strongly orientation and spatial-frequency selective but with different preferences and bandwidths. Neurons show different amounts of surround suppression and texture modulation.



## Distributions of single neuron properties in some processing stages of hierarchical neural networks quantitatively approximately those in macaque V1

Because single artificial neurons in some of the V1 candidate models respond similarly to single neurons in macaque V1, we next sought to quantify these individual artificial neurons and compare to macaque V1 as a whole. For example, it is possible that some V1 neuronal subpopulations are completely absent in some candidate V1 models or that the V1 model neuronal populations are biased towards some response types. Specifically, we compared the distributions of response properties in the V1 models with the respective empirical distributions measured in macaque V1. We focused on 22 single neuron response properties that we extracted from published V1 studies (Cavanaugh et al., 2002; De Valois, Albrecht, et al., 1982; De Valois, Yund, et al., 1982; Freeman et al., 2013; Ringach et al., 2002; P. H. Schiller et al., 1976; Ziemba et al., 2016) and replicated the corresponding experiments in each V1 candidate model (Figure 3A and Supplementary Figure 2). Each in silico experiment consisted of estimating an empirical model neuronal distribution on randomly sampling the same number of artificial V1 neurons included in the empirical biological distribution of the corresponding biology experiment. This procedure was then repeated 1,000 times to estimate the uncertainty with respect to candidate V1 model neuronal sampling (methods). We considered the following response properties: preferred orientation, circular variance (CV), orientation selectivity, orientation half-bandwidth, ratio of orthogonal and preferred responses (Orth./Pref.), ratio between CV and orientation half-bandwidth, difference between the Orth./Pref. and CV, peak SF, SF selectivity, SF bandwidth, grating summation field, surround diameter, surround suppression index, texture modulation index, absolute texture modulation index, F1/F0 ratio, texture selectivity, texture sparseness, texture variance ratio, maximum DC response, maximum texture response, and maximum noise response. Details on how these are calculated can be found in the Methods section.

We found that some V1 models had distributions of some response properties that closely approximated those reported in macaque V1 not only in their range but also their distributional shape (Figure 3A and Supplementary Figure 2). We defined a normalized distribution similarity score as  $(1 - KS_c^{M-E}) / (1 - KS_c^{E-E})$ , where  $KS_c^{M-E}$  is the ceiled Kolmogorov-Smirnov (KS) distance between the empirical model distribution and the empirical biological distribution and  $KS_c^{E-E}$  is an estimate of the expected ceiled KS distance between different biology experiments (methods). A low score means that the model distribution does not match the biological distribution while a score of 1 means that the model distribution is indistinguishable from the biological distribution considering experimental variability. We note that the similarity score ceiling is not limited by the model approach here. Instead, it depends on, and is thus limited by, the biological sample size and number of bins of the empirical biological distribution: smaller number of neurons and bins tend to lead to lower ceilings and therefore decrease the range of scores for different models. As expected, response properties with model distributions that were qualitatively similar to the biological distributions had scores close to 1 while those that show large differences between the distributions achieved lower scores (Figure 3A and Supplementary Figure 2). To quantify how well a V1 model approximates macaque V1 at the single neuron level according to these response properties, we pooled the property scores in seven groups (Figure 3B; orientation tuning, spatial frequency tuning, receptive-field size, surround modulation, texture modulation, response selectivity, and response

magnitude). Then, we averaged the scores within each group, and, finally, averaged the seven group scores, obtaining a V1 Composite Properties score (Supplementary Figure 3). Note that this composite score should not be taken as a final way to assess a V1 model's match to primate V1, but only as a summary of the match to the measures that are dominant in the field, weighted as outlined above.

Since the model V1 Composite Properties match score depends on the distribution of its individual V1 neurons, the composite score also depends on all of the factors outlined in the previous section: the choice of base hierarchical neural network, the choice of FoV, and the choice of model layer to take as the model V1 (Supplementary Figure 3). For example, for V1 models derived from the same base model and FoV, similarity scores vary considerably with the choice of model layer to assign as V1 (Supplementary Figure 3A). In particular, we report here that the scores for different V1 properties show interesting dependencies on these choices that motivates future work (Supplementary Figure 3A,B). While some V1 candidate models achieved very high similarity scores for multiple response properties, no candidate V1 model tested here was able to match macaque V1 in all the response properties (Figure 3B shows scores for the V1 model with highest V1 Composite Properties score).

In summary, we report here that some candidate V1 models contained within hierarchical network models of the ventral stream have single artificial neurons that have similar responses to those of single neurons in macaque V1 and that also approximate V1 at the population level. In spite of this, no model in the large pool of candidate V1 models analyzed (n=736) was able to match macaque V1 along all the response properties.

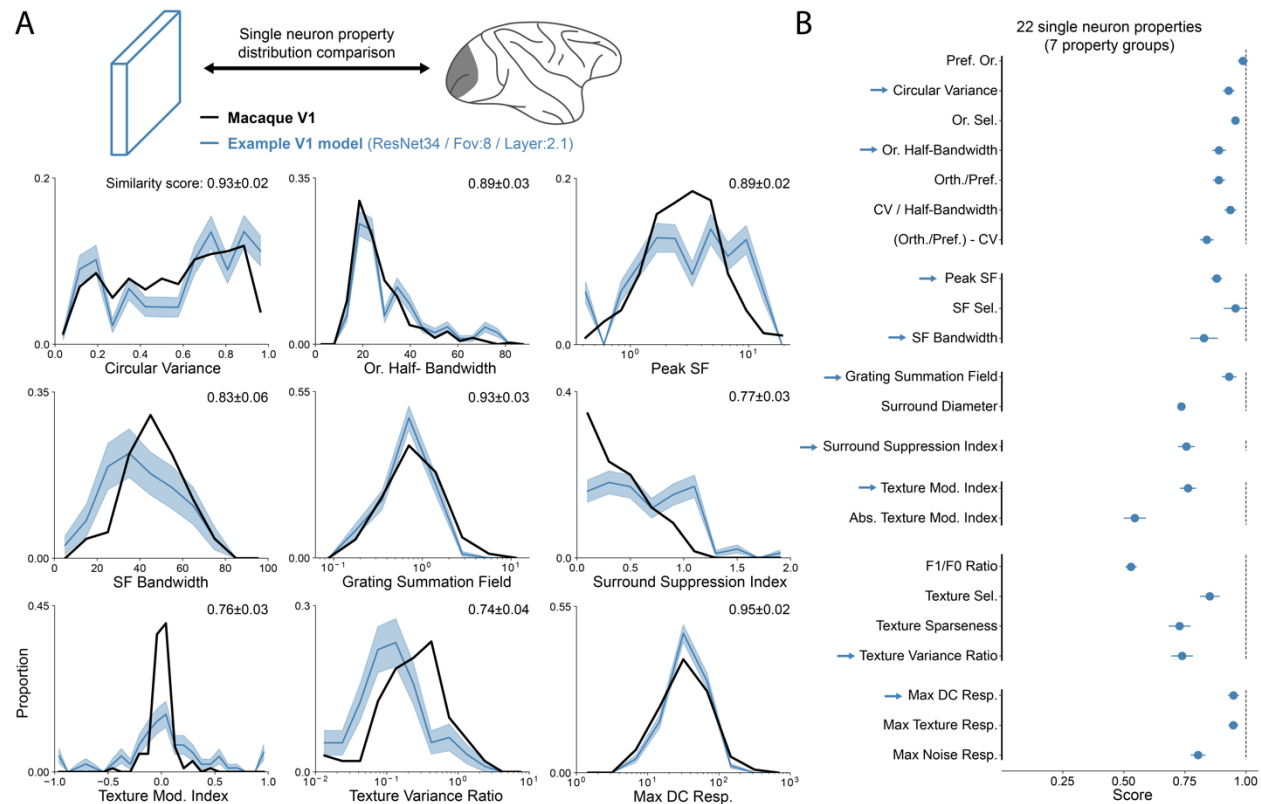


**Figure 3. Distributions of single neuron response properties in a candidate V1 model approximately match those in macaque V1.** **A.** Distributions of nine example response properties in macaque V1 (from published studies, black line) and a V1 model (ResNet34-FoV8-Layer2.1, same as in Figure 1). Model distributions are obtained by performing in silico experiments, thick blue line is the mean over 1,000 experiments and the shaded region is the SD. All the 22 response property distributions are shown in Supplementary Figure 2. Normalized similarity scores are shown in each plot at the top right corner. **B.** Similarity scores for the 22 single neuron response properties for the same V1 model (errorbars represent mean and SD). Arrows indicate the response properties shown in **A**. Response properties are displayed in seven groups: orientation tuning, spatial frequency tuning, receptive-field size, surround modulation, texture modulation, response selectivity, and response magnitude.

## Different response property similarity scores provide complementary information about a model's similarity to V1

Why is no single model able to match the distributions of all V1 response properties? One hypothesis is that there are some response properties for which that property is never found in the small family of feedforward, ImageNet trained ANN models considered here. An alternative hypothesis is that all of the biological V1 properties measured thus far are explained by this model family, but that they are found in different model layers rather than being expressed in a single population of putative V1 neurons. Distinguishing between these alternatives is important because it could guide future model architectural choices.

To disambiguate these two hypotheses, we first looked at the distributions of all the property similarity scores over all the V1 models (Figure 4A). The distributions of scores for different properties varied considerably in their ranges: some properties, such as the preferred orientation and maximum DC responses had very high scores for most models, while others, such as the grating summation field and texture variance ratio, had very

broad distributions of scores. This is also illustrated by the large spread of score medians over the different properties, ranging from 0.41 for the surround diameter to 0.96 for the preferred orientation. Still, despite the large differences between the distributions of scores, for most properties, at least on the candidate V1 models had a very high score. In particular, only three properties had a maximum score lower than 0.95 (surround suppression index, texture modulation index, and texture sparseness), and none lower than 0.9. In sum, the family of ANN-derived multi-stage models we considered is already capable of virtually identically matching all of the 22 biological V1 response properties studied here.

We then looked at the correlations between different property scores across all V1 candidate models. Correlations between scores of different properties showed great variability (Figure 4B). We found that some pairs of properties such as the ratio of orthogonal and preferred responses and circular variance were highly correlated over V1 models – models that tend to match one property also tend to match the other. (Figure 4B top left,  $r=0.87$ ). Scores of other pairs such as the surround suppression index and spatial-frequency bandwidth are not correlated at all (Figure 4B top middle,  $r=0.06$ ). Most interestingly, we found that some pairs of properties scores were anti-correlated (Figure 4B top right, grating summation field and absolute texture modulation index,  $r=-0.59$ ). That is, V1 models that tend to capture one property, tend to do worse on the other property. We also found that scores of properties that belong to the same group, i.e., that relate to similarly named phenomena, were significantly more correlated than scores of properties of different groups ( $r_{\text{same}}=0.33\pm0.28$  vs  $r_{\text{different}}=0.11\pm0.23$ ; t-test,  $t=4.23$ ,  $p\text{-value}=1.2\text{E-}4$ ). However, when considering all the properties, scores were on average weakly correlated (Figure 4C).

Next, we analyzed whether the property scores could be explained by simple model parameters. As previously mentioned, within the same hierarchical base model, some property scores depend on model parameters such the layer depth and FoV (Supplementary Figure 3). When we consider all the models, we observed some interesting relationships between property scores and model parameters (Supplementary Figure 4A). These relationships, however, were not always aligned. For example, both the receptive field size and the texture modulation property scores vary with the model's theoretical receptive field and layer depth but were optimal for different values (Supplementary Figure 4A). How much variance in the different property scores can be explained by simple model properties? We performed a sequential ANOVA to identify which model parameters contributed the most to explain variance in the property scores, and quantify how much of the variance in scores can be attributed to the model parameters (Supplementary Figure 4B; model parameters considered were the model total depth, FoV, layer depth, theoretical receptive field, layer type, and number of neurons). Theoretical receptive field was the most important model parameter in explaining the variance in scores of four property groups (orientation tuning, spatial frequency tuning, receptive field size, and response magnitude) as well as in the V1 Composite Properties. On the other hand, layer depth was the model parameter that explained the most variance for surround modulation, texture modulation and response selectivity properties. In total, the six model parameters accounted for 65% of the variance in the V1 Composite Properties scores.

These results show that within the set of V1 candidate models analyzed here, there is at least one model that approximates each of the macaque V1 property distributions reasonably well (score over 0.9). However, since scores of different properties are on average weakly correlated and some pairs of property scores are, in fact, anti-correlated, no model was able to simultaneously match all of the V1 empirical distributions. This suggests that different properties reflect different aspects of model similarity to V1, which are not necessarily aligned, and that there may exist constraints in the model architecture (e.g. feedforward only except for the CORnet-S architecture) limiting the ability to fully approximate biological V1. Finally, a large fraction of the variance in the scores can be explained by simple model parameters such as the theoretical receptive field and layer depth.

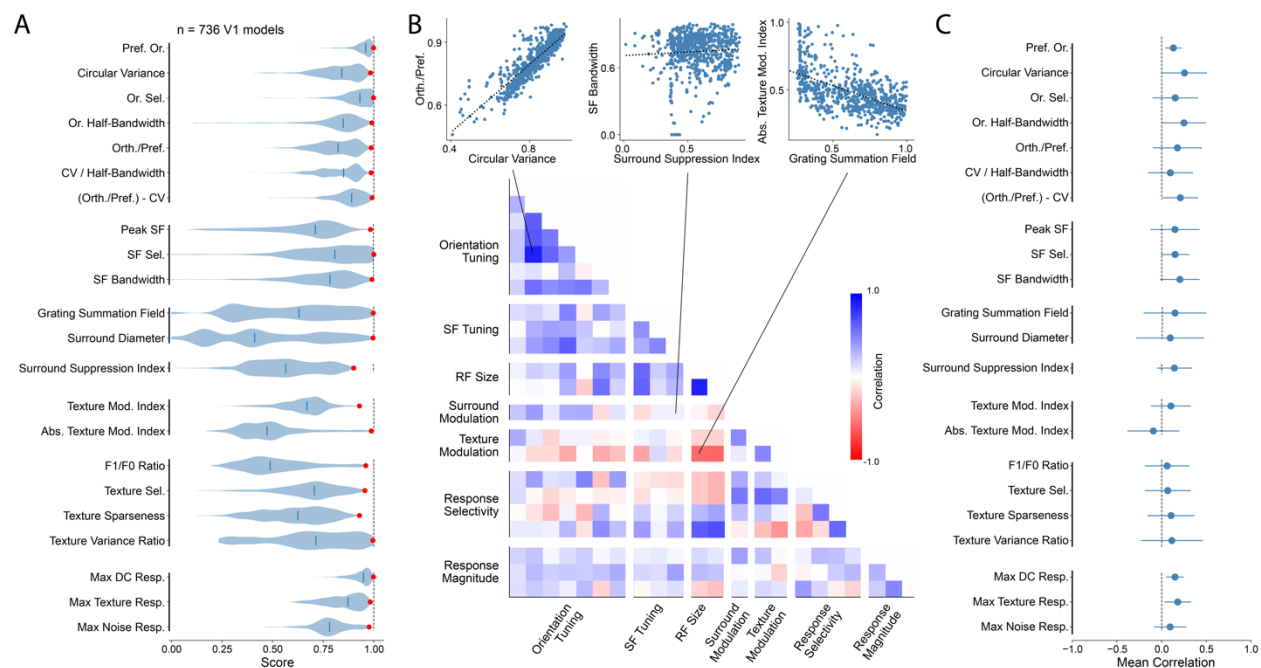


**Figure 4. Single neuron response properties similarity scores are on average weakly correlated across V1 candidate models.** **A.** Violin plots show the distributions of similarity scores over 736 ANN V1 models for the 22 single neuron response properties. Thick blue lines indicate the median of each distribution and the red dots the maximum. There is significant variability in the individual property scores across models. **B.** Top, scatter plots comparing three pairs of different response property similarity scores. Left, similarity scores of circular variance and ratio between orthogonal and preferred orientation responses are positively correlated. Middle, similarity scores of surround suppression index and spatial frequency bandwidth are not correlated. Right, similarity scores of absolute texture modulation index and grating summation field are negatively correlated. Bottom, pair-wise correlations between the 22 single neuron response property scores grouped in the seven groups (correlations are calculated across all models). Lines connect to the corresponding scatter plots on top. **C.** Mean pair-wise correlations for each response property with all the others (errorbars represent mean and SD). On average single neuron response property scores are weakly correlated.

## Single neuron properties similarity scores correlate with similarity scores derived from standard explained variance metrics

How do the V1 property scores described here compare to more conventional methods that evaluate the model's similarity to V1 (Cadena et al., 2019; Dapello et al., 2020) To address this question, we calculated for each V1 candidate model how well it explained



stimulus driven responses of V1 neurons using a standard neural predictivity methodology based on partial least square regression (PLS) (Helland, 2006; Schrimpf et al., 2018; Yamins et al., 2014). We used a neuronal dataset containing extracellular recordings from 102 single-units while presenting naturalistic textures and noise images which had been originally published in a study analyzing texture modulation in macaque V1 and V2 (Freeman et al., 2013). The dataset consisted of stimulus-evoked responses to 315 images (20 repetitions and averaged over 100ms). For each model, neurons were mapped to the V1 neuronal population linearly using a PLS regression model with 25 components. Model predictions were evaluated using a 10-fold cross-validation strategy. V1 explained variance was then normalized by the neuronal internal consistency to arrive at specific V1 explained variance benchmarks that we consider next.

Across all V1 models, we found that the neuronal explained variance benchmark was strongly correlated with the V1 Composite Properties score outlined above (Figure 5A,  $r=0.64$ ,  $p\text{-value}=2.2e-86$ ). On average, individual property groups were also correlated with V1 explained variance using PLS regression, though there was considerable variability across groups (Figure 5B,C;  $r=0.31\pm0.11$ , mean and SD). Increasing the number of property groups averaged gradually improves the alignment of the V1 component property scores with explained variance (Figure 5B). This correlation was not exclusive to V1 explained variance using PLS regression, since it was present when using other metrics on this same neural data set. Response property distribution similarity scores were also correlated with explained variance using single neuron mapping (choosing the single neuron in the model that best predicts a single macaque V1 neuron;  $r=0.52$ ) (Arend et al., 2018), and with representational similarity metrics such as representational dissimilarity matrix (RDM;  $r=0.34$ ) (Kriegeskorte et al., 2008), and center kernel alignment (CKA;  $r=0.25$ ) (Kornblith, Norouzi, Lee, & Hinton, 2019) that also do not involve fitting model features. Considering all the different metrics tested, we found that orientation tuning and response magnitude were the V1 component property scores that least aligned with V1 explained variance benchmark (Figure 5C). Finally, the alignment between the V1 Composite Properties scores and the V1 explained variance was not an artifact of the way that the individual property scores were first averaged in groups (Supplementary Figure 5). When directly calculating the mean of the 22 individual property scores, the correlation with V1 explained variance persisted ( $r=0.59$ ), even when removing the seven response properties that overlap with the neuronal dataset used for determining the explained variance ( $r=0.46$ ).

In sum, we find that the V1 property scores are partially aligned with more conventional methods for evaluating a candidate V1 model's ability to predict V1 responses. While this result is not entirely surprising, it serves as an important sanity-check, showing that there is signal in the response property distributions similarity scores for benchmarking models in how well they explain V1. Alternatively, this result can also be interpreted as at least a partial validation of regression-based methods for evaluating neural predictivity of ANN-based models, in spite of their reliance on a fitting step (see Discussion).



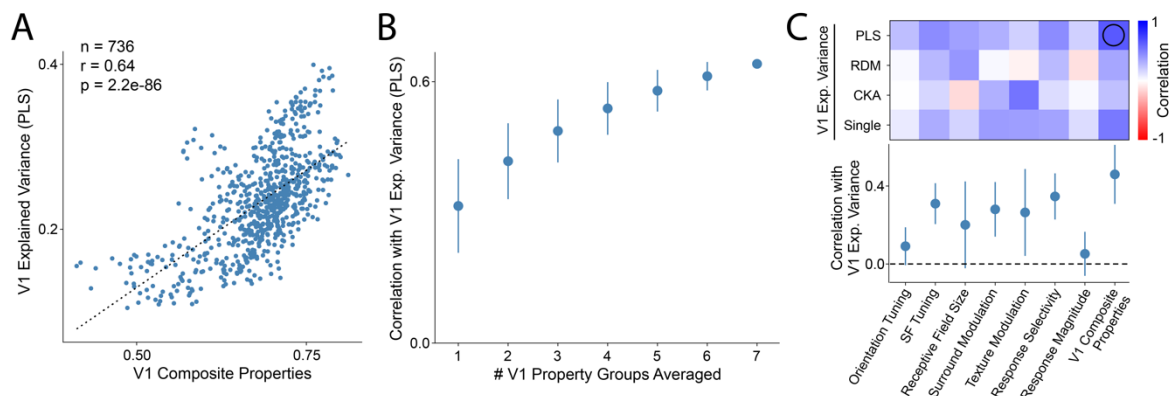


**Figure 5. Single neuron response property similarity scores correlate with the V1 model's ability to predict neuronal responses using standard measures (cross-validated explained variance).** **A.** Comparison of model's ability to explain variance in macaque V1 responses in a neuronal dataset (Freeman, Ziemba et al 2013) using PLS regression and V1 composite properties scores (across 736 V1 models). Model's cross-validated explained variance is positively correlated with the V1 composite properties scores. **B.** Averaging over an increasingly higher number of property group scores improves correlation with V1 explained variance. **C.** Top, correlation of V1 property groups and composite properties scores with different V1 explained variance metrics (PLS, RDM, CKA, and single neuron mapping). Open black circle indicates the correlation shown in **A**. Bottom, same as above but showing the mean and SD across the different explained variance metrics.

## Hierarchical models that have more brain-like V1 stages are more aligned with primate object recognition behavior

While better models of primate V1 is an important goal in and of itself, our larger goal is to do this in the service of multi-scale, multi-stage models of the ventral visual stream and visually-driven behavior. Thus, we next asked, do multi-stage artificial neural network models that better align with biological V1 also tend to better align with biological behavior? Building on prior work, we here focused on primate core object recognition behavior. Specifically, when assessed via batteries of core object recognition tasks, humans and monkeys show highly aligned difficulty and confusion patterns at the object- and image-level (R. Rajalingham, Schmidt, & DiCarlo, 2015; Rishi Rajalingham et al., 2018). That is, humans and monkeys not only show similar levels of accuracy in a visual categorization task, but they also reliably show the same patterns of successes and failures when scored at the grain of object categories (pooling over subjects and images of the same category) or at the grain of individual images (pooling over subjects), and those reliable patterns can thus be used to assess the biological veracity of any image-computable model at the behavioral level. Indeed, while some hierarchical neural network models accurately match typical primate patterns of object confusion, they do not yet match those patterns at the image-level (Rishi Rajalingham et al., 2018) and some models do better than others (Schrimpf et al., 2018). Thus, we here asked if hierarchical models with intermediate layers that better match V1, i.e. more brain-like V1-layers, also better match human (and monkey) core object recognition patterns of behavior using these same prior benchmarks.

Each hierarchical model with a specific FoV was here taken as a candidate multi-scale, multi-stage model of the ventral stream and its resultant behavior. For each of these candidate ventral stream models ( $n=52$ , 13 base models with 4 different FoVs), we chose the layer that best approximated macaque V1 according to the layer's single neuron Composite Properties score (above). We then performed psychophysical experiments on

each model to evaluate how well the overall model aligned with human image-level behavior in classifying a set of naturalistic synthetic images using the same benchmarks and methods described in prior work (Rishi Rajalingham et al., 2018), which we briefly summarize here. Images consisted of objects belonging to 24 categories (100 images per category) displayed at different positions, orientations, and sizes, and overlaid on a random natural background. For each hierarchical model, we trained a behavioral decoder to classify the images using the activations of the model's penultimate layer (top layer before the 1000-way ImageNet class probability layer). Training and testing of the behavioral decoder were done using a cross-validation strategy.

We found that human image-level confusion consistency of the hierarchical neural network models was strongly correlated with the model's V1 Composite Properties score of its best internal layer (Figure 6A,  $r=0.79$ ,  $p\text{-value}=2.4\text{e-}12$ ). We also found reducing the number of V1 property groups that are included (averaged) in the V1 properties composite score tended to reduce the correlation between model V1 match scores and model behavioral consistency with humans (Figure 6B). This suggests that all V1 properties already measured are at least partially important to understanding V1's role in supporting recognition behavior. However, we also found considerable variability between the correlation of single response property scores and behavioral consistency, with response selectivity and response magnitude showing little to no correlation, and orientation tuning being anti-correlated (Figure 6C). Despite object-level behavioral consistencies being considerably higher than image-level consistencies, the alignment between V1 property scores and behavioral consistency was very similar for all the different behavioral metrics (Figure 6C). Finally, the V1 explained variance on the neuronal dataset previously described was considerably less correlated with behavioral consistency than the V1 composite properties scores (Figure 6C).

In sum, we found that hierarchical neural networks with intermediate layers that better match macaque V1, also better explain primate object recognition behavior. This demonstrates an empirical, across-scale linkage between single neuron response properties and object recognition behavior: multi-stage neural network models constructed with an internal V1 layer that better matches the distribution of individual V1 biological neuronal properties tends to also better match biological behavior.

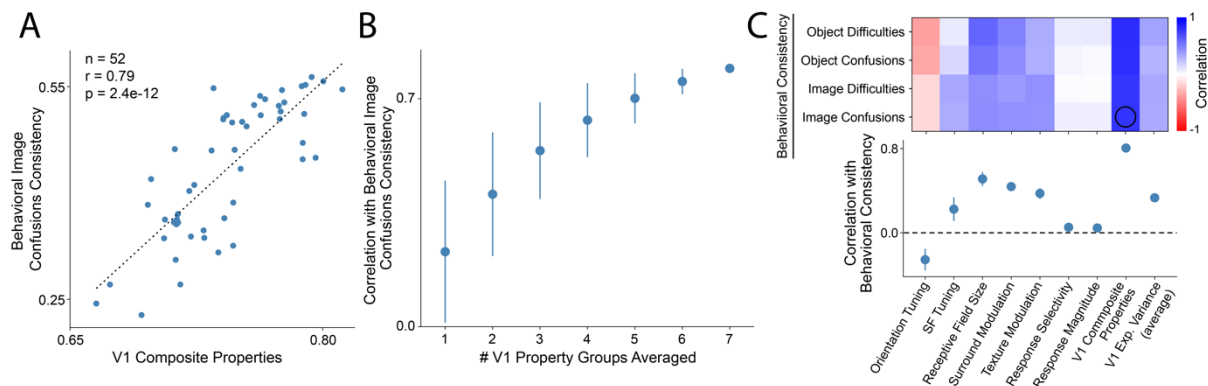


**Figure 6. Hierarchical models with internal processing stages (layers) that better match macaque V1 at the single neuron level have output behavioral patterns that are better matched to human behavioral patterns. A.** Comparison of human object recognition behavioral consistency and V1 composite properties scores for 52 hierarchical models. Behavioral consistency represents the alignment between the models' output (i.e. model "behavior") and humans performing a two-alternative forced choice object recognition task at the image-level (I2n metric, image-level normalized confusion patterns, see (Rishi Rajalingham et al., 2018)). For each hierarchical neural network, the internal model layer with the highest V1 composite properties score was chosen. **B.** Decreasing the number of V1 response property groups considered in the overall V1 score reduces the behavioral consistency (the plot in A shows the result when all seven property groups are included). **C.** Top, correlation of V1 property group scores, V1 composite properties scores and V1 explained variance (average of metrics) with behavioral consistency metrics with varying granularity: object difficulties (O1), object confusion patterns (O2), image normalized difficulties (I1n), and image normalized confusion patterns (I2n). Open black circle indicates the correlation shown in A. Bottom, same as above but showing the mean and SD across the different behavioral consistency metrics.

## How do the candidate V1 models tested here compare with classical models of V1?

As previously mentioned, no V1 model derived from the current ventral stream model family was able to completely match macaque V1 along all the single neuron response properties considered. We wondered whether a classical neuroscientific model of V1 might do better, given that such models were constructed largely guided by the kinds of empirical results used to compute that score here. While those classical models are limited in that they were not constructed to bridge all the way to behavior, their match to V1 is nonetheless an important reference in determining future ventral stream model efforts. Answering how good the classical neuroscientific model is turns out to be non-trivial as there is no standard, agreed-upon classical neuroscientific model. For example, Cadena et al. showed that a task-optimized ANN outperformed one variant of the classical linear-nonlinear model of V1 based on a Gabor filter bank (GFB) followed by simple- and complex-cell nonlinearities in predicting responses in macaque V1 (Cadena et al., 2019). However, Dapello, Marques et al. more recently showed that constraining the GFB parameters with empirical data (i.e. a different variant of the classical model) substantially improves its ability to explain V1 response variance (Dapello et al., 2020).

To answer our original reference question (above) and to help clarify the current state of the art in image-computable V1 models, we implemented both of these V1 classical models: a data-constrained classical V1 model consisting of a GFB (J. P. Jones & Palmer, 1987), simple- and complex-cell (Adelson & Bergen, 1985) nonlinearities and a simple divisive normalization stage (Carandini, Heeger, & Movshon, 1997; Heeger, Simoncelli, & Movshon, 1996) (Classical V1 model variant 1; see Methods), and the GFB model used in Cadena et al. (Classical V1 model variant 2). We then compared both of these classical

model variants with the candidate V1 models derived from hierarchical ANNs considered in this study (above). Using the V1 properties scores developed here, we found that the classical V1 model variant 1 outperformed all the ANN-derived V1 models by a wide margin, but that many of the ANN-derived models outperformed the Classical V1 model variant 2 (Figure 7A,C; V1 Composite Properties scores: optimized classical V1 model  $0.90 \pm 0.03$ , GFB in Cadena et al.  $0.70 \pm 0.03$ , best V1 model based on hierarchical ANNs  $0.81 \pm 0.03$ ).

Interestingly, when using the V1 neuronal explained variance on the neuronal dataset described before, we found that a V1 model derived from an adversarially-trained hierarchical ANN (Engstrom, Ilyas, Santurkar, & Tsipras, 2019; Madry, Makelov, Schmidt, Tsipras, & Vladu, 2019) was better than all the others (Figure 7B,C; average V1 explained variance: adversarially-trained ANN  $0.278 \pm 0.005$ , optimized classical V1 model  $0.247 \pm 0.005$ , GFB in Cadena et al.  $0.181 \pm 0.005$ , best standard ImageNet-trained ANN-based model  $0.220 \pm 0.005$ ). This result had already been reported by some of the authors (Dapello et al., 2020) but here we extend to other metrics.

In sum, using the V1 Composite Properties Score, the classical V1 model variant 1 is a better match to macaque V1 than all the ANN-derived V1 models explored in this study. The same holds true even when averaging both the V1 Composite Properties scores with the V1 explained variance (Figure 7C, bottom). However, none of the models we tested was able to completely approximate V1, particularly in predicting the neuronal responses in the dataset considered. Together, these results suggest that there is still considerable room to improve current models of macaque V1.

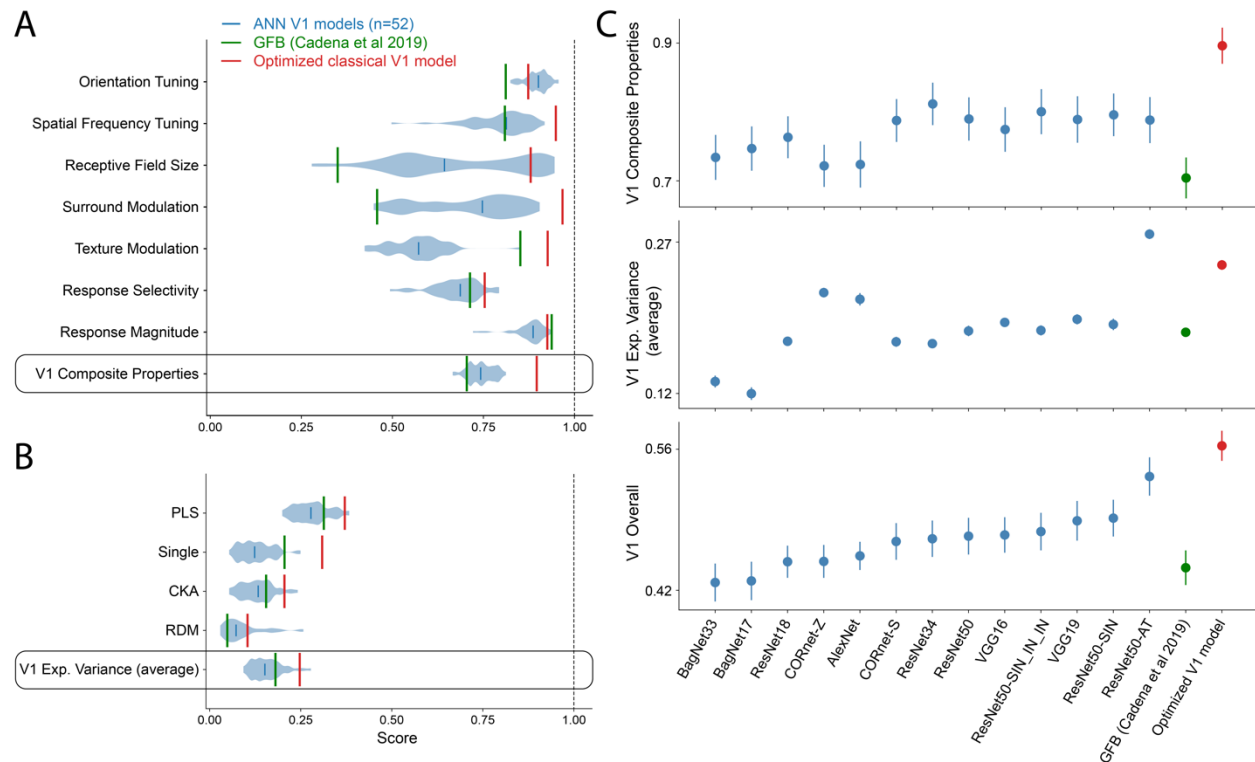


**Figure 7. An optimized classical neuroscientific V1 model outperforms V1 models based on hierarchical neural network models in approximating macaque V1. A.** Violin plots represent distributions of scores for the seven groups of V1 properties as well as the V1 Composite Properties for the most V1-like layer in 52 hierarchical models (13 base models with 4 FoVs). Green line represents the GFB model used in Cadena et al 2019 as the classical V1 model control. Red line represents an optimized neuroscientific model of V1 with a GFB, simple- and complex-cell nonlinearities, and divisive normalization stage. **B.** Same as in **A** but for V1 explained variance using different metrics (PLS regression, single neuron mapping, CKA, and RDM) and the average of all metrics. **C.** V1 Composite Properties score (top), average explained variance (middle), and V1 overall score (bottom) for the best combination of layer and FoV for each base hierarchical model and the two classical V1 models. V1 models based on hierarchical ANNs are sorted according to their V1 overall score. An optimized classical V1 model outperforms all hierarchical models on the V1 Composite Properties scores and overall and is only surpassed by an adversarially-trained model in explained variance. The adversarially-trained ResNet50 outperformed all other models in V1 explained variance.

## Discussion

In this work, we evaluated whether hierarchical neural networks of artificial neurons are accurate, multi-scale, multi-stage models of the primate ventral visual stream, bridging between the properties of individual cells and object recognition behavior. While it was known that these models are moderately accurate in predicting neuronal responses in ventral stream areas using regression methods, how their single neurons relate to single neurons in the brain had not to our knowledge been studied before. Specifically, our goals were: (1) to evaluate whether single neurons in V1 models based on hierarchical neural network models were functionally similar to single neurons in macaque V1; (2) to test whether the distributions of multiple single neuron response properties in the V1-layers of these hierarchical models matched those in macaque V1; and (3) to ask if hierarchical models with better V1 layers (i.e. more similar to macaque V1 at the single neuron level) were also more similar to primate behavior at their output level. Our results confirmed that not only single neurons in hierarchical models of the primate ventral visual stream have response characteristics that are surprisingly similar to their biological counterparts,



but also that the distributions of response properties in some of their V1-layers approximately match those in macaque V1. Furthermore, we observed that hierarchical models with more brain-like V1-layers, were also more aligned with human object recognition behavior. Together with prior work, these results suggest that the hierarchical neural network models that we built here are reasonably accurate, multi-scale models of the primate ventral visual stream and its support of object recognition behavior. Indeed, these models are multi-scale in that they could now be used to assess the predicted behavioral effects of altering individual V1 single neurons. Nevertheless, these results also show that none of these models is perfect and they provide pointers to future modeling improvement avenues.

## **Multi-scale, hierarchical models of the primate ventral stream**

Some hierarchical artificial neural networks have achieved unparalleled accuracy in predicting visual neuronal responses in low- (Cadena et al., 2019) and high-level (Yamins et al., 2014) visual cortical areas, as well as object recognition behavior (Rishi Rajalingham et al., 2018), making them the current best scientific hypotheses of the neural processing mechanisms at work along the primate ventral stream. However, these models are far from perfect. For instance, they cannot completely account for all the explainable response variance in the neural and behavioral data (Schrimpf et al., 2018). Furthermore, these models tend to be largely feedforward, making it hard for them to model the recurrent processing dynamics in the ventral stream; though we and others have recently started to address this (Kietzmann, Spoerer, Sörensen, Cichy, & Hauk, 2019; Kubilius et al., 2019; Nayebi et al., 2018; Tang et al., 2018).

In this study, we focused on another critical aspect that the leading hierarchical ANNs still lack: if any such model claims to be a multi-scale, multi-stage, neurally-mechanistic model of the primate ventral visual stream it must have alignment with cortical areas at the level of individual neurons. Specifically, past studies using multi-stage ANN models to explain single neuronal responses in primate ventral stream areas have used the model neurons as an encoding basis (Cadena et al., 2019; Yamins et al., 2014) or with representational similarity analysis (Cadieu et al., 2014; Güçlü & van Gerven, 2015; Khaligh-Razavi & Kriegeskorte, 2014). While the first approach accurately fits and predicts individual biological neuronal responses, it does so by combining the activity of thousands of model neurons. Similarly, the latter approach compares the representational spaces between a neuronal population in the model and a neuronal population in the brain. In both cases, single neurons in the model are not explicitly mapped to individual neurons in ventral stream areas. Here, we make the first steps towards hierarchical models of the primate ventral stream that are truly multi-scale, multi-stage and thus can bridge between properties of individual cells in intermediate model levels to visually-guided behavior.

Our approach consisted in hypothesizing a one-to-one mapping at the level of single neurons between macaque V1 and a processing stage in each hierarchical model which we refer to as a candidate V1 model. Then, by performing a series of *in silico* experiments replicating neurophysiological studies, we characterized single neuron responses in the model V1-layer and compared them to those in the macaque V1. This approach presents multiple advantages when compared to existing methods for evaluating V1 similarity. The



first, and most obvious one, is the one-to-one single neuron mapping which ensures the alignment at the level of single neurons between the candidate V1 model and the corresponding cortical area. This, in turn, dispenses the standard regression fitting procedure, which can give rise to situations of under- and over-fitting depending on the availability and variability of the data. Another important advantage of the approach used here is the improved interpretability of the response property distribution similarity scores. Conventional methods for evaluating a model's match to neuronal data only provide an answer to the question "How much variance does the model explain?". Our approach, on the other hand, gives a more detailed description of "Which aspects of the neuronal responses are explained by the V1 model and which aspects a not?" In addition, it does so using a language familiar to the visual neuroscience community by relying on single neuron response properties extensively used in V1 neurophysiology. Which leads us to the final advantage of the proposed methodology, its reliance on published primate V1 studies, meaning that the approach presented here can be further extended to include other aspects of V1 processing without requiring new biological experiments. Other single neuron response properties such as those related to color tuning (Horwitz & Hass, 2012), figure-ground modulation (Lamme, 1995), and border ownership (Zhou, Friedman, von R., & von der Heydt, 2000) can also be analyzed to give an even more complete evaluation of the model's similarity to V1 at the level of single neurons.

## **Modeling macaque V1 with hierarchical neural network models at the level of single neurons**

In general, hierarchical neural network models provided moderately accurate models of macaque V1 at the level of single neurons. This result extends prior work that used these models to predict neuronal responses in macaque V1 using regression-based methods (Cadena et al., 2019; Dapello et al., 2020). However, we report that no model was able to simultaneously match all the 22 single neuron response property distributions (highest V1 composite properties score was  $0.81 \pm 0.03$ ). This was not due to some individual response properties being impossible to match by this model family since there was always at least one model that approximately matched each of the V1 single neuron response property distributions (similarity score larger than 0.9). Instead, the reason for the failure to match all of the response properties is likely due to the limitations of the model architectures we considered. Scores for some response properties varied with particular model properties and in several cases in non-optimal ways.

Not surprisingly, we found that V1 similarity at the level of single neurons was somewhat aligned with V1 explained variance using conventional approaches. Still, this alignment was not perfect suggesting that each individual comparison benchmark reflects only a particular, and incomplete, aspect of V1 similarity. This is true for each of the single neuron property distribution similarity scores, which only evaluate V1 similarity in a very specific phenomenon, as well as for the V1 explained variance which is limited by the type of stimuli and size of the dataset. This observation reinforces the idea that, to best evaluate the ability of a model to explain brain processing, one should consider multiple and varied benchmarks (Schrimpf et al., 2018, 2020).

Unlike Cadena et al., we found that V1 models derived from hierarchical ANNs underperformed in explaining V1 neuronal phenomena when compared to an optimized

classical neuroscientific model. This was true for both the single neuron property distribution similarity scores and the V1 explained variance (except for the adversarially-trained model). While there are several differences in the neuronal datasets and the fitting procedures used in the two studies, we believe that the main reason for this apparent difference in results is due the differences in the classical V1 model. Indeed, when we used an off-the-shelf classical V1 model identical to the one used in the Cadena et al. study, we qualitatively replicated their result in that we also found that many ANN-derived V1 models matched the biological V1 better than that classical V1 model. The fact that we also found that an optimized classical V1 model still outperforms (on average) all of the tested ANN-derived models has important implications since it suggests that current hierarchical ANN architectures are not yet the best model class for approximating macaque V1.

So how can we improve current models of V1? Our results suggest several possibilities. First, by tweaking with the architectural parameters of these hierarchical neural networks, such as the kernel sizes of the convolutions, it may be possible to remove the observed sub-optimal interactions and, thus, improve V1 similarity. In addition, we can expand the model space by including new circuit motifs inspired by neurobiology, such as local recurrence. The implementation of these types of architectural changes could potentially be guided by the V1 similarity scores described here. Another alternative is exploring other task-optimization procedures for training the model weights. Similarly to another recent study (Dapello et al., 2020), we found that adversarially-trained models had the highest V1 neuronal explained variance. Exploring other types of data augmentation during training may result in even stronger V1 similarity. Finally, the higher V1 similarity scores of the classical neuroscientific model suggests that there may be opportunities in merging that type of mathematically elegant model with task-optimized neural networks. Such an approach has been successfully used to improve the adversarial robustness of neural network models for object recognition (Dapello et al., 2020). However, we must remain wary of the possibility that the set of hierarchical models considered may not allow to completely approximate macaque V1.

## **Bridging from single neuron properties to behavioral phenomena**

By evaluating the ability of hierarchical neural network models to match macaque V1 at the single neuron level, we were able to produce models that offer a bridge from the level of single neuron properties in the first visual cortical area all the way to object recognition behavioral phenomena. The alignment of V1 similarity with behavioral consistency in these hierarchical models suggests that object recognition behavior is derived, at least in part, from low-level visual processing in V1. This is in agreement with the recent result showing that V1 similarity also correlates with robustness to image perturbations (Dapello et al., 2020). Together, these results all point towards the same conclusion: that working to build better models of low-level visual processing has tangible payoffs in improving models of visual behavior.

Going forward, we believe that the approach used here will lead to a deeper understanding of the neural processing along the ventral visual stream and its support of visual object recognition and other visually driven behaviors. By building even more accurate, multi-scale, multi-stage models of the primate ventral stream, we will begin to

uncover how specific cellular mechanisms at work along the multiple ventral stream areas contribute to different aspects of visual intelligence.

## **Acknowledgments**

We thank J. Anthony Movshon and Corey M. Ziemba for access to the V1 neural dataset, and Joel Dapello for adding some ANN models used in this study to the Brain-Score platform. This work was supported by the PhRMA Foundation Postdoctoral Fellowship in Informatics (T.M), the Semiconductor Research Corporation (SRC) and DARPA (M.S., J.J.D.), the Massachusetts Institute of Technology Shoemaker Fellowship (M.S.), Office of Naval Research grant MURI-114407 (J.J.D.), the Simons Foundation grant SCGB-542965 (J.J.D.), the MIT-IBM Watson AI Lab grant W1771646 (J.J.D.)

## **Author Contributions**

T.M. and J.J.D. designed the study. T.M., M.S., and J.J.D. designed the analysis. T.M. and M.S. implemented the analysis. T.M. developed the classical V1 model. T.M. and J.J.D. wrote the paper.

# References

- Adelson, E. H., & Bergen, J. R. (1985). Spatiotemporal energy models for the perception of motion. *Journal of the Optical Society of America A, Optics and Image Science*, 2(2), 284–299. <https://doi.org/10.1364/JOSAA.2.000284>
- Arend, L., Han, Y., Schrimpf, M., Bashivan, P., Kar, K., Poggio, T., ... Boix, X. (2018). Single units in a deep neural network functionally correspond with neurons in the brain: preliminary results. *CBMM Memo*, (093), 1–23.
- Bair, W., Cavanaugh, J. R., & Movshon, J. A. (2003). Time course and time-distance relationships for surround suppression in macaque V1 neurons. *Journal of Neuroscience*, 23(20), 7690–7701. <https://doi.org/23/20/7690> [pii]
- Bashivan, P., Kar, K., & DiCarlo, J. J. (2019). Neural population control via deep image synthesis. In *Science* (Vol. 364). <https://doi.org/10.1126/science.aav9436>
- Brendel, W., & Bethge, M. (2019). Approximating CNNs with Bag-of-local-Features models works surprisingly well on ImageNet, 1–15.
- Cadena, S. A., Denfield, G. H., Walker, E. Y., Gatys, L. A., Tolias, A. S., Bethge, M., & Ecker, A. S. (2019). Deep convolutional models improve predictions of macaque V1 responses to natural images Author summary. *PLoS Computational Biology*, 1–28. <https://doi.org/10.12751/g-node.2e31e3>
- Cadiou, C. F., Hong, H., Yamins, D. L. K., Pinto, N., Ardila, D., Solomon, E. A., ... DiCarlo, J. J. (2014). Deep Neural Networks Rival the Representation of Primate IT Cortex for Core Visual Object Recognition. *PLoS Computational Biology*, 10(12). <https://doi.org/10.1371/journal.pcbi.1003963>
- Carandini, M., Heeger, D. J., & Movshon, J. A. (1997). Linearity and normalization in simple cells of the macaque primary visual cortex. *The Journal of Neuroscience : The Official Journal of the Society for Neuroscience*, 17(21), 8621–8644.
- Cavanaugh, J. R., Bair, W., & Movshon, J. A. (2002). Nature and Interaction of Signals From the Receptive Field Center and Surround in Macaque V1 Neurons. *Journal of Neurophysiology*, 88(5), 2530–2546. <https://doi.org/10.1152/jn.00692.2001>
- Chollet, F. (2015). Keras.
- Dapello, J., Marques, T., Schrimpf, M., Geiger, F., Cox, D. D., & DiCarlo, J. J. (2020). Simulating a primary visual cortex at the front of CNNs improves robustness to image perturbations. *NeurIPS*, 1–30. <https://doi.org/10.1101/2020.06.16.154542>
- De Valois, R. L., Albrecht, D. G., & Thorell, L. G. (1982). Spatial Frequency Selectivity of Cells in Macaque Visual Cortex. *Vision Research*, 22, 545–559.
- De Valois, R. L., Yund, E. W., & Hepler, N. (1982). The orientation and direction selectivity of cells in macaque visual cortex. *Vision Research*, 22, 531–544.
- DiCarlo, J. J., & Cox, D. (2007). Untangling invariant object recognition. *Trends in*

- Cognitive Sciences*, 11(8), 333–341. <https://doi.org/10.1016/j.tics.2007.06.010>
- DiCarlo, J. J., Zoccolan, D., & Rust, N. C. (2012). How Does the Brain Solve Visual Object Recognition? *Neuron*, 73(3), 415–434. <https://doi.org/10.1016/j.neuron.2012.01.010>
- Engstrom, L., Ilyas, A., Santurkar, S., & Tsipras, D. (2019). Robustness (Python Library).
- Fabre-Thorpe, M., Richard, G., & Thorpe, S. J. (1998). Rapid categorization of natural images by rhesus monkeys. *NeuroReport*, 9(2), 303–308. <https://doi.org/10.1097/00001756-199801260-00023>
- Felleman, D. J., & Van Essen, D. C. (1991). Distributed hierarchical processing in the primate cerebral cortex. *Cerebral Cortex*, 1(1), 1–47.
- Freeman, J., Ziemba, C. M., Heeger, D. J., Simoncelli, E. P., & Movshon, J. A. (2013). A functional and perceptual signature of the second visual area in primates. *Nature Neuroscience*, 16(7), 974–981. <https://doi.org/10.1038/nn.3402>
- Geirhos, R., Rubisch, P., Michaelis, C., Bethge, M., Wichmann, F. A., & Brendel, W. (2019). ImageNet-trained CNNs are biased towards texture; increasing shape bias improves accuracy and robustness. In *ICLR* (pp. 1–22).
- Güçlü, U., & van Gerven, M. A. J. (2015). Deep Neural Networks Reveal a Gradient in the Complexity of Neural Representations across the Brain's Ventral Visual Pathway. *The Journal of Neuroscience*, 35(27), 10005–10014. <https://doi.org/10.1523/JNEUROSCI.5023-14.2015>
- He, K., Zhang, X., Ren, S., & Sun, J. (2016). Deep Residual Learning for Image Recognition. In *CVPR* (pp. 1–12).
- Heeger, D. J., Simoncelli, E. P., & Movshon, J. A. (1996). Computational models of cortical visual processing. *Proceedings of the National Academy of Sciences of the United States of America*, 93(2), 623–627. <https://doi.org/10.1073/pnas.93.2.623>
- Helland, I. (2006). Partial Least Squares Regression. In *Encyclopedia of Statistical Sciences*. American Cancer Society. <https://doi.org/https://doi.org/10.1002/0471667196.ess6004.pub2>
- Horwitz, G. D., & Hass, C. A. (2012). Nonlinear analysis of macaque V1 color tuning reveals cardinal directions for cortical color processing. *Nature Neuroscience*, 15(6), 913–919. <https://doi.org/10.1038/nn.3105>
- Jones, H. E., Grieve, K. L., Wang, W., & Sillito, A. M. (2001). Surround suppression in primate V1. *Journal of Neurophysiology*, 86(4), 2011–2028. <https://doi.org/10.1152/jn.2001.86.4.2011>
- Jones, J. P., & Palmer, L. A. (1987). The two-dimensional spatial structure of simple receptive fields in cat striate cortex. *Journal of Neurophysiology*, 58(6), 1187–1211. <https://doi.org/10.1152/jn.1987.58.6.1187>



- Kapadia, M. K., Ito, M., Gilbert, C. D., & Westheimer, G. (1995). Improvement in visual sensitivity by changes in local context: Parallel studies in human observers and in V1 of alert monkeys. *Neuron*, 15(4), 843–856. [https://doi.org/10.1016/0896-6273\(95\)90175-2](https://doi.org/10.1016/0896-6273(95)90175-2)
- Kar, K., Kubilius, J., Schmidt, K., Issa, E. B., & DiCarlo, J. J. (2019). Evidence that recurrent circuits are critical to the ventral stream’s execution of core object recognition behavior. *Nature Neuroscience*. <https://doi.org/10.1038/s41593-019-0392-5>
- Khaligh-Razavi, S. M., & Kriegeskorte, N. (2014). Deep Supervised, but Not Unsupervised, Models May Explain IT Cortical Representation. *PLoS Computational Biology*, 10(11). <https://doi.org/10.1371/journal.pcbi.1003915>
- Kietzmann, T. C., Spoerer, C. J., Sörensen, L. K. A., Cichy, R. M., & Hauk, O. (2019). Recurrence is required to capture the representational dynamics of the human visual system, 116(43). <https://doi.org/10.1073/pnas.1905544116>
- Kornblith, S., Norouzi, M., Lee, H., & Hinton, G. (2019). Similarity of Neural Network Representations Revisited.
- Kriegeskorte, N. (2015). Deep Neural Networks: A New Framework for Modeling Biological Vision and Brain Information Processing. *Annual Review of Vision Science*, 1(1), 417–446. <https://doi.org/10.1146/annurev-vision-082114-035447>
- Kriegeskorte, N., Mur, M., Ruff, D. A., Kiani, R., Bodurka, J., Esteky, H., ... Bandettini, P. A. (2008). Matching Categorical Object Representations in Inferior Temporal Cortex of Man and Monkey. *Neuron*, 60(6), 1126–1141. <https://doi.org/10.1016/j.neuron.2008.10.043>
- Krizhevsky, A., Sutskever, I., & Geoffrey E., H. (2012). ImageNet Classification with Deep Convolutional Neural Networks. In *NIPS* (pp. 1097–1105). <https://doi.org/10.1109/5.726791>
- Kubilius, J., Schrimpf, M., Kar, K., Hong, H., Majaj, N. J., Rajalingham, R., ... DiCarlo, J. J. (2019). Brain-Like Object Recognition with High-Performing Shallow Recurrent ANNs. *NeurIPS*, (NeurIPS), 1–12.
- Kubilius, J., Schrimpf, M., Nayebi, A., Bear, D., Yamins, D. L. K., & DiCarlo, J. J. (2018). CORnet: Modeling the Neural Mechanisms of Core Object Recognition. *BioRxiv*, 1–9. <https://doi.org/10.1101/408385>
- Lamme, V. A. F. (1995). The Neurophysiology of Figure-Ground Segregation in Primary Visual Cortex. *The Journal of Neuroscience*, 15(2), 1605–1615.
- Madry, A., Makelov, A., Schmidt, L., Tsipras, D., & Vladu, A. (2019). Towards Deep Learning Models Resistant to Adversarial Attacks. *ArXiv*, 1–28.
- Mishkin, M., Ungerleider, L. G., & Macko, K. A. (1983). Object vision and spatial vision: two cortical pathways. *Trends in Neurosciences*, 6(C), 414–417. [https://doi.org/10.1016/0166-2236\(83\)90190-X](https://doi.org/10.1016/0166-2236(83)90190-X)



- Nassi, J. J., Lomber, S. G., & Born, R. T. (2013). Corticocortical Feedback Contributes to Surround Suppression in V1 of the Alert Primate. *Journal of Neuroscience*, 33(19), 8504–8517. <https://doi.org/10.1523/JNEUROSCI.5124-12.2013>
- Nayebi, A., Bear, D., Kumbhani, J., Kar, K., Ganguli, S., Sussillo, D., ... Yamins, D. L. K. (2018). Task-Driven Convolutional Recurrent Models of the Visual System. *ArXiv*, 1–14.
- Nurminen, L., Merlin, S., Bijanzadeh, M., Federer, F., & Angelucci, A. (2018). Top-down feedback controls spatial summation and response amplitude in primate visual cortex. *Nature Communications*, 9(1). <https://doi.org/10.1038/s41467-018-04500-5>
- Paszke, A., Gross, S., Massa, F., Lerer, A., Bradbury, J., Chanan, G., ... Chintala, S. (2019). PyTorch: An imperative style, high-performance deep learning library. *NeurIPS*.
- Rajalingham, R., Schmidt, K., & DiCarlo, J. J. (2015). Comparison of Object Recognition Behavior in Human and Monkey. *Journal of Neuroscience*, 35(35), 12127–12136. <https://doi.org/10.1523/JNEUROSCI.0573-15.2015>
- Rajalingham, Rishi, Issa, E. B., Bashivan, P., Kar, K., Schmidt, K., & DiCarlo, J. J. (2018). Large-scale, high-resolution comparison of the core visual object recognition behavior of humans, monkeys, and state-of-the-art deep artificial neural networks. *The Journal of Neuroscience*, 38(33), 7255–7269. <https://doi.org/10.1523/JNEUROSCI.0388-18.2018>
- Richards, B. A., Lillicrap, T. P., Beaudoin, P., Bengio, Y., Bogacz, R., Christensen, A., ... Kording, K. P. (2019). A deep learning framework for neuroscience. *Nature Neuroscience*, 22(11), 1761–1770. <https://doi.org/10.1038/s41593-019-0520-2>
- Ringach, D. L., Shapley, R. M., & Hawken, M. J. (2002). Orientation selectivity in macaque V1: diversity and laminar dependence. *The Journal of Neuroscience*, 22(13), 5639–5651. <https://doi.org/20026567>
- Saxe, A., Nelli, S., & Summerfield, C. (2021). If deep learning is the answer, what is the question? *Nature Reviews Neuroscience*, 22(1), 55–67. <https://doi.org/10.1038/s41583-020-00395-8>
- Sceniak, M. P., Ringach, D. L., Hawken, M. J., & Shapley, R. (1999). Contrast's effect on spatial summation by macaque V1 neurons. *Nature Neuroscience*, 2(8), 733–739. <https://doi.org/10.1038/11197>
- Schiller, P. H., Finlay, B. L., & Volman, S. F. (1976). Quantitative studies of single-cell properties in monkey striate cortex. III. Spatial Frequency. *Journal of Neurophysiology*, 39(6), 1334–1351. <https://doi.org/10.1152/jn.1976.39.6.1352>
- Schiller, Peter H, Finlay, L., & Volman, F. (1976). Quantitative Studies of Single-Cell Properties in Monkey Striate Cortex. II. Orientation Specificity and Ocular Dominance. *Journal of Neurophysiology*, 39(6), 1320–1333. <https://doi.org/018.030.060.187>
- Schrimpf, M., Kumbhani, J., Hong, H., Majaj, N. J., Rajalingham, R., Issa, E. B., ...

- DiCarlo, J. J. (2018). Brain-Score: Which Artificial Neural Network for Object Recognition is most Brain-Like? *BioRxiv*, 1–9. <https://doi.org/10.1101/407007>
- Schrimpf, M., Kubilius, J., Lee, M. J., Ratan Murty, N. A., Ajemian, R., & DiCarlo, J. J. (2020). Integrative Benchmarking to Advance Neurally Mechanistic Models of Human Intelligence. *Neuron*, 1–11. <https://doi.org/10.1016/j.neuron.2020.07.040>
- Serre, T. (2019). Deep Learning: The Good, the Bad, and the Ugly. *Annual Review of Vision Science*, 5(1), 399–426. <https://doi.org/10.1146/annurev-vision-091718-014951>
- Simonyan, K., & Zisserman, A. (2015). Very Deep Convolutional Networks for Large-Scale Image Recognition. In *ICLR* (pp. 1–14). <https://doi.org/10.2146/ajhp170251>
- Skottun, B. C., De Valois, R. L., Grosof, D. H., Movshon, J. A., Albrecht, D. G., & Bonds, A. B. (1991). Classifying simple and complex cells on the basis of response modulation. *Vision Research*, 31(7–8), 1079–1086. [https://doi.org/10.1016/0042-6989\(91\)90033-2](https://doi.org/10.1016/0042-6989(91)90033-2)
- Tang, H., Schrimpf, M., Lotter, W., Moerman, C., Paredes, A., Ortega Caro, J., ... Kreiman, G. (2018). Recurrent computations for visual pattern completion. *Proceedings of the National Academy of Sciences*, 115(35), 8835–8840. <https://doi.org/10.1073/pnas.1719397115>
- Yamins, D. L. K., & DiCarlo, J. J. (2016). Using goal-driven deep learning models to understand sensory cortex. *Nature Neuroscience*, 19(3), 356–365. <https://doi.org/10.1038/nn.4244>
- Yamins, D. L. K., Hong, H., Cadieu, C. F., Solomon, E. A., Seibert, D., & DiCarlo, J. J. (2014). Performance-optimized hierarchical models predict neural responses in higher visual cortex. *Proceedings of the National Academy of Sciences*, 111(23), 8619–8624. <https://doi.org/10.1073/pnas.1403112111>
- Zhou, H., Friedman, H. S., von R, der H., & von der Heydt, R. (2000). Coding of border ownership in monkey visual cortex. *Journal of Neuroscience*, 20(17), 6594. <https://doi.org/10.1523/JNEUROSCI.2797-12.2013>
- Ziomba, C. M., Freeman, J., Movshon, J. A., & Simoncelli, E. P. (2016). Selectivity and tolerance for visual texture in macaque V2. *Proceedings of the National Academy of Sciences*, 113(22), E3140–E3149. <https://doi.org/10.1073/pnas.1510847113>

# Methods

## Hierarchical neural network models of the primate ventral visual stream

In this study we considered 13 pre-trained artificial neural networks (ANNs) to build multi-scale, hierarchical models of the primate ventral visual stream. All models were accessed via the Brain Score platform (Schrimpf et al., 2018). The models considered were the following: AlexNet (Krizhevsky et al., 2012), VGG16 and VGG19 (Simonyan & Zisserman, 2015), CORnet-Z and CORnet-S (Kubilius et al., 2019, 2018), ResNet18, ResNet34 and ResNet50 (He et al., 2016), bagnet17 and bagnet33 (Brendel & Bethge, 2019), ResNet50-SIN and ResNet50-SIN\_IN\_IN, which are trained on a stylized ImageNet dataset (Geirhos et al., 2019), and an adversarially-trained ResNet50 with a  $\|\delta\|_\infty = 4/255$  constraint (Engstrom et al., 2019). All models were implemented with Pytorch (Paszke et al., 2019) except the VGG models which used Keras (Chollet, 2015). For each ANN base model, we built multiple V1 models using a three-step commitment as described in the Results section for a total of 736 V1 models.

## Empirical macaque V1 single neuron property distributions

To evaluate the ability of hierarchical neural network models of explaining macaque V1 at the single neuron level, we extracted from the literature the empirical distributions of 22 single neuron response properties in macaque V1. Since some response properties depend on eccentricity, we chose distributions that corresponded to foveal neurons (eccentricities less than 5deg). With a few exceptions, the distributions were directly taken from the paper figures using an assistance digital tool (WebPlotDigitizer). The distributions were rounded to integers and normalized to ensure the same total number of neurons reported in the paper. The single neuron response properties from Ringach et al. 2002 are publicly available online (<http://ringachlab.net>). The single neuron response properties from Freeman, Ziemba et al. 2013 and Freeman, Ziemba et al. 2016 were calculated from the neuronal responses generously provided by the authors.

## In silico neurophysiology experiments

To calculate the V1 model distributions for all the single neuron response properties, we performed in silico neurophysiology experiments that attempted to approximate the biological experiments carried out in the V1 studies. However, to facilitate their implementation, we made a methodological simplification that does not alter our results. Since all the layers of the ANNs considered here were convolutional layers, neurons respond identically at all the locations of the visual space. Due to this, instead of randomly sampling neurons with receptive fields (RF) spread along the whole visual space, we fixed a single location to record where we centered the stimuli (deviated from the center of gaze by 0.5deg on each orientation resulting at an eccentricity of 0.7deg).

We first estimated the functional receptive field (RF) for all the neurons in the V1 model by presenting small gratings (0.33deg diameter, 3cpd spatial frequency, four orientations and two opposing phases) in a grid with a spacing of 0.25deg, and averaging the responses for each position. We then selected all the neurons that had their RF centers aligned (within 0.15deg) with the stimulus location. Depending on the single neuron response property, we presented the respective stimulus set. In total we used four different stimulus sets: gratings for orientation tuning (8 phases, 12 orientations, 4 spatial frequencies, 3 diameters per spatial frequency), gratings for spatial frequency tuning (8

phases, 6 orientations, 22 spatial frequencies, 1 diameter), gratings for size tuning (8 phases, 6 orientations, 4 spatial frequencies, 12 diameters), naturalistic textures and noise images (for both types 15 texture families and 15 samples per family).

Response properties for each neuron were calculated from the responses to the stimuli following the methodology used in the original study. Below are the 22 response properties paired with their respective studies.

- De Valois, Yund, et al., 1982: preferred orientation
- Ringach et al., 2002: circular variance (CV), orientation selectivity, orientation half-bandwidth, Orth./Pref., ratio between CV and orientation half-bandwidth, difference between the Orth./Pref. and CV, maximum DC response, F1/F0 ratio
- P. H. Schiller et al., 1976: SF selectivity, SF bandwidth
- De Valois, Albrecht, et al., 1982: peak SF
- Cavanaugh et al., 2002: grating summation field, surround diameter, surround suppression index
- Freeman et al., 2013: texture modulation index, absolute texture modulation index, maximum texture response, and maximum noise response
- Ziemba et al., 2016: texture selectivity, texture sparseness, texture variance ratio

We sampled the same number of artificial neurons as those sampled in the empirical biological distribution of the corresponding experimental study. We then calculated the histogram of the in silico experiment using the same bins as in the empirical biological distribution. We computed a similarity score  $(1 - KS_c^{M-E})$  where  $KS_c^{M-E}$  is the ceiled Kolmogorov-Smirnov (KS) distance between the empirical model distribution and the empirical biological distribution. The ceiled KS distance is calculated as the ratio between the actual KS distance and the maximum possible KS distance given the shape of the empirical biological distribution. We normalized the similarity score by an estimate of the similarity between empirical biological distributions  $(1 - KS_c^{E-E})$  calculated by bootstrapping the empirical biological distribution. Thus, the final normalized distribution similarity score is calculated as  $(1 - KS_c^{M-E}) / (1 - KS_c^{E-E})$ . This procedure was repeated 1,000 times, each time with a different sample of artificial neurons, to estimate the uncertainty with respect to the V1 model neuronal sampling. Values reported are mean and SD.

## Classical V1 models

We implemented two variants of a classical V1 model containing a Gabor filter bank (GFB). The Classical V1 model variant 1 consisted of a variation to the V1 model front-end added to ANNs in Dapello, Marques et al., 2020. The original model contained a GFB constrained by empirical biological distributions, simple- and complex-cell nonlinearities, and a neuronal stochasticity generator. Here, we removed the neuronal stochasticity generator and added a divisive normalization stage which normalizes the output of the nonlinearities by  $(1 + k_D D)$ , where  $k_D$  is a constant that controls the amount of suppression and  $D$  is the output of the nonlinearity convolved with a Gaussian of size  $\sigma_D$ .  $k_D$  and  $\sigma_D$  are defined separately per channel and their distributions are constrained by data. The model has three hyper-parameters, one controlling the relationship between the spatial frequency and size of the Gabors, one controlling the spatial scale of the local division, and another controlling the magnitude of the local division. We searched over 80

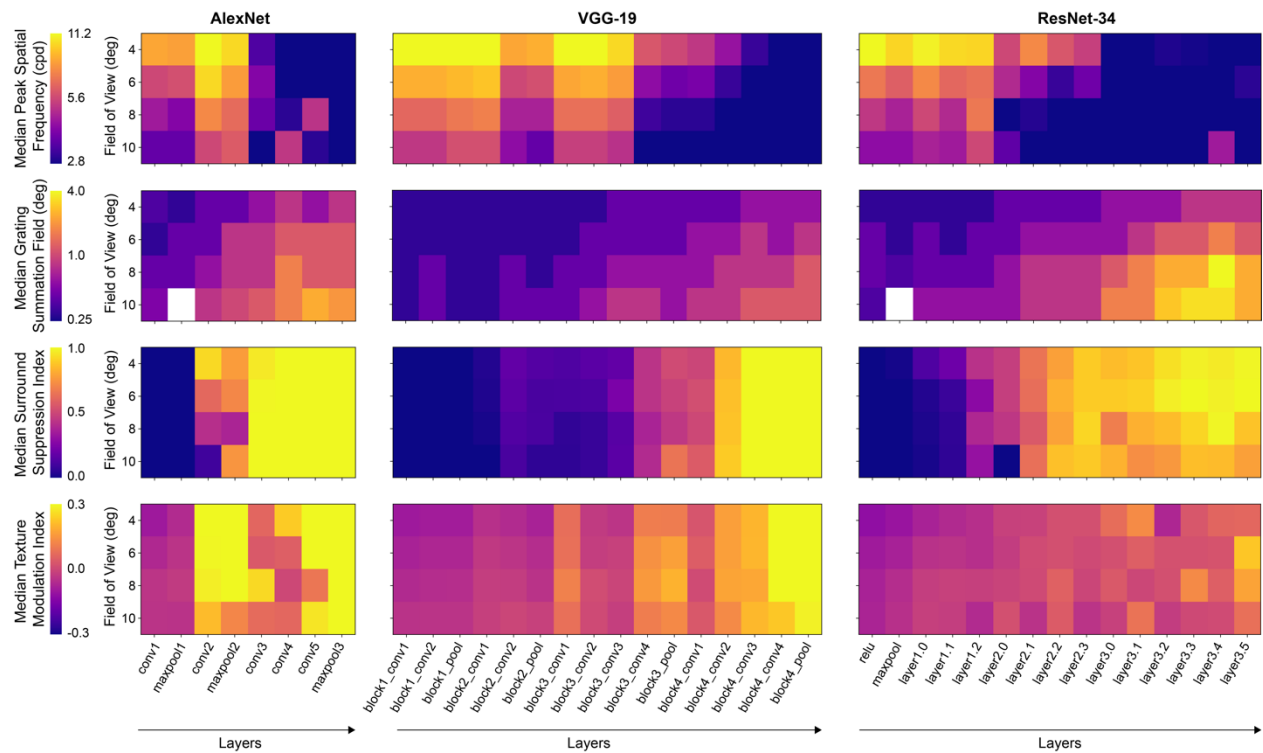
combinations of these parameters and chose the optimal model according to the V1 Composite Property score. The Classical V1 model variant 2 was implemented according to Cadena et al., 2019.

### **Code availability**

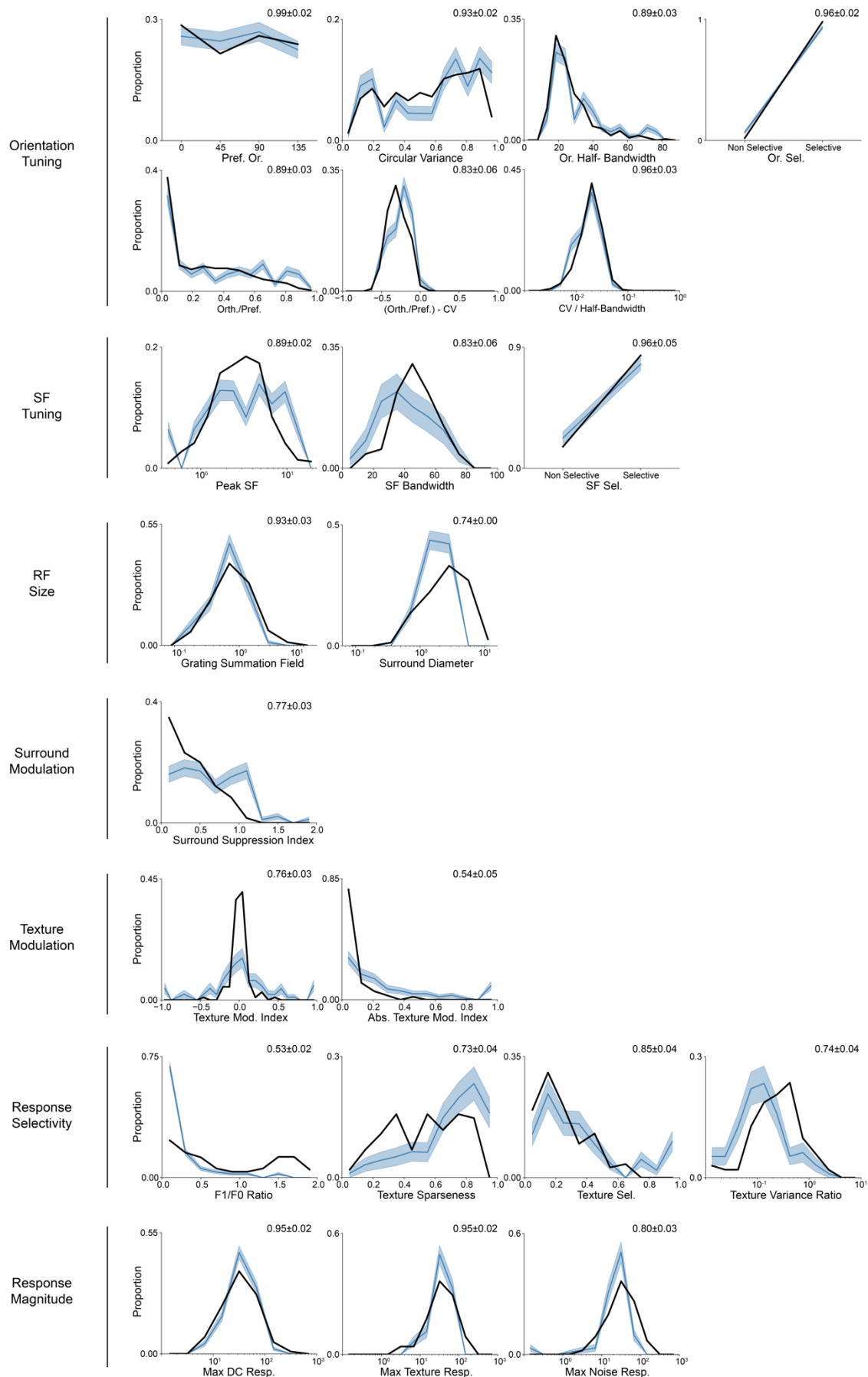
Code for calculating the 22 single neuron response properties, evaluating ANNs on the V1 response property similarity scores, V1 explain variance, and behavioral consistency is available at the Brain-Score repository <https://github.com/brain-score/brain-score>



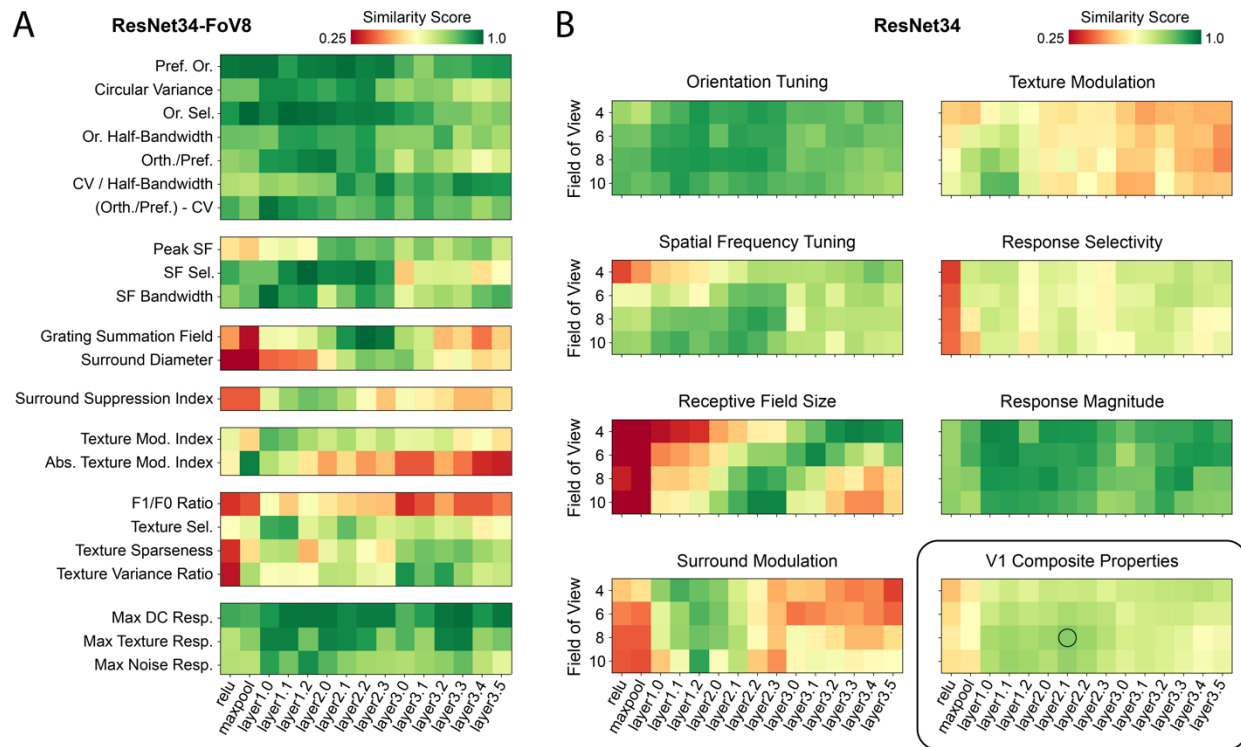
# Supplementary Material



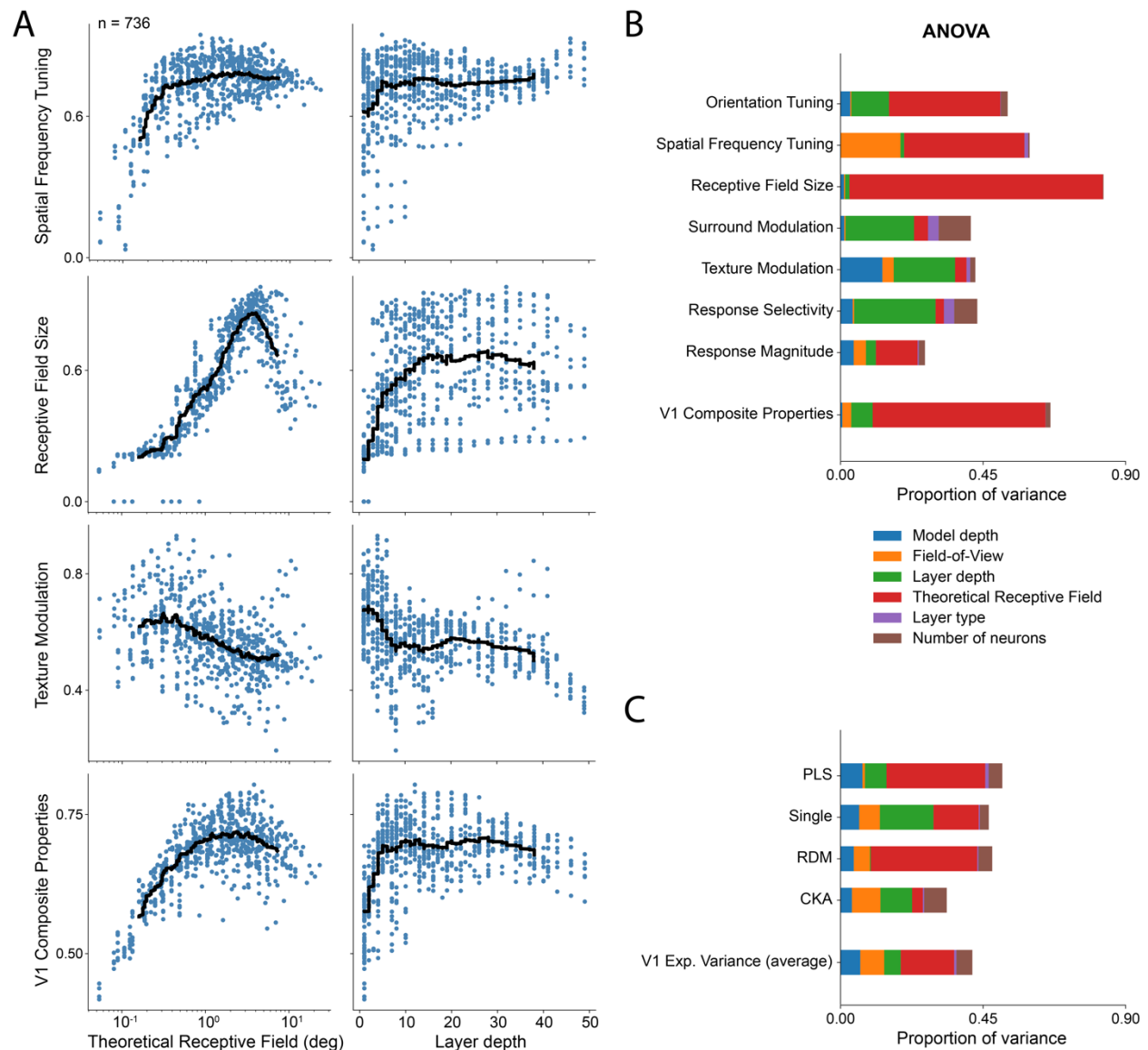
**Supplementary Figure 1. Response properties of V1 models vary with base model, field-of-view, and layer.** Medians of four example response properties for the V1 models resulting from three base hierarchical models (AlexNet, VGG-19, and ResNet34). From top to bottom, peak spatial frequency, grating summation field, surround suppression index, and texture modulation index. These examples illustrate how different response properties vary with the three steps of the model commitment: choice of base model, choice of FoV, and choice of V1-layer.



**Supplementary Figure 2. Comparison of distributions of response properties between example V1 model and macaque V1** Distributions for all the 22 single neuron response properties in macaque V1 (from published studies, black line) and an example V1 model (ResNet34-FoV8-layer2.1; obtained by performing in silico experiments in the model, thick blue line is the mean over 1,000 experiments and the shaded region is the SD). Normalized similarity score, shown in each plot at the top right corner. Response properties are organized in seven groups: orientation tuning, spatial frequency tuning, receptive field size, surround modulation, texture modulation, response selectivity, and response magnitude.

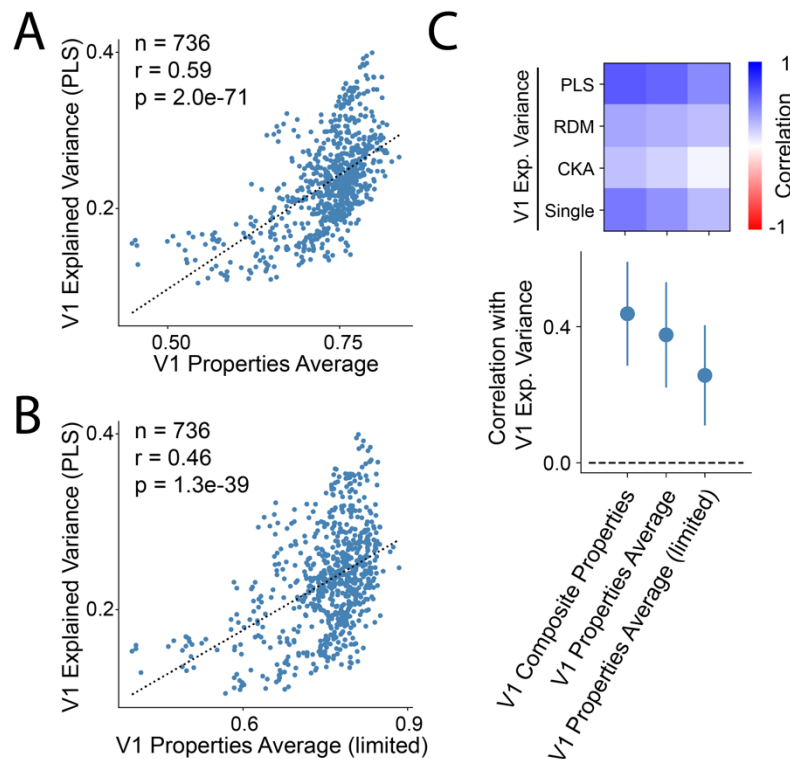


**Supplementary Figure 3. Response properties similarity scores for V1 models based on the ResNet34 base model.** **A.** Similarity scores for the 22 V1 response properties for all the layers of the ResNet34 with a FoV of 8 degrees. No layer is able to simultaneously approximate the distributions of all the response properties in macaque V1. Different response properties have different optimal layers. For example, grating summation field similarity score peaks at layer 2.2, while for texture modulation the score peaks at earlier layers (layer 1.0). **B.** Average scores for the seven response property groups as well as the overall V1 composite properties scores for all the V1 models based on the ResNet34 base model (all layers and FoV). For some property groups scores, there is a strong interaction between the layer and FoV. For example, for the receptive field size scores, the best models are either intermediate layers with large input FoV or higher layers with small input FoV. Best overall V1 model based on the ResNet34 base model is the one with a FoV of 8 degrees and layer 2.1 (model represented with a circle in the V1 composite properties scores and is the same model as in Figure 2, and 3).



**Supplementary Figure 4. Model properties account for the majority of the variance in the response property scores.** **A.** Similarity scores for three example response property groups (spatial frequency tuning, receptive field size, and texture modulation) and V1 composite properties as a function of the model's theoretical receptive field size and layer depth for all the V1 ANN-based models ( $n=736$ ). Black line is the moving average (window of 100). Depending on the response properties, over all the models, V1 similarity scores vary with model properties. For example, receptive field size similarity scores are optimal for models with theoretical receptive field sizes of  $\sim 4$  degrees. **B.** Sequential ANOVA for determining how much variance in the property scores can be explained by model properties excluding interactions (see methods). For the V1 composite properties scores, most of the variance (65.1%) can be explained by six model properties: model depth, FoV, layer depth, theoretical receptive field, layer type and number of neurons. The theoretical receptive field corresponds to the fraction of the visual input that neurons can be influenced by (in degrees) and does not correspond to the receptive field size as determined by the *in silico* electrophysiology experiments. Layer depth is defined as the cumulative number of non-linear processing stages until the model layer and model depth is the total number of non-linear processing stages in the ANN. Layer type can be either convolution followed by a ReLU or a maxpool operation. Theoretical receptive field size is the model property that explains most variance in the V1 composite and property groups scores, followed by the layer depth. **C.** Same as B but for different V1 explained variance metrics in a given neuronal dataset.





**Supplementary Figure 5. Correlation of model's property distribution similarity scores with explained variance is robust.** **A.** Similar to Figure 5 A but V1 property scores are averaged directly along the 22 response properties and not pre-pooled in groups. Comparison of model's ability to explain variance in macaque V1 responses in a neuronal dataset (Freeman, Ziemba et al 2013) using PLS regression and V1 properties average scores (across 736 ANN V1 models). Model's explained variance is positively correlated with the V1 properties average scores. **B.** Same as **A** but discarding the response property scores that are calculated using the same stimuli and neuronal responses that are used for the V1 explained variance: texture modulation index, absolute texture modulation index, texture selectivity, texture sparseness, variance ratio, maximum texture response, and maximum noise response. There is still a significant correlation between the V1 explained variance and the average of the limited pool of non-overlapping response property scores (15 response properties). **C.** Top, correlation of the three distinct ways to pool the V1 property scores (composite, average, and limited average) with different V1 explained variance metrics (PLS, RDM, CKA, and single neuron mapping). Bottom, same as above but showing the mean and SD across the different explained variance metrics.